10-5-2017

The Application of Regenerative Braking System to the Commercial Hybrid Vehicles with All-Wheel Drive System

Yi Zhang
University of Windsor

The Application of Regenerative Braking System to the Commercial Hybrid Vehicles with All-Wheel Drive System

By

Yi Zhang

A Thesis

Submitted to the Faculty of Graduate Studies
through the Department of Mechanical, Automotive & Materials Engineering
in Partial Fulfillment of the Requirements for
the Degree of Master of Applied Science

at the University of Windsor

Windsor, Ontario, Canada

2017

The Application of Regenerative Braking System to the Commercial Hybrid Vehicles with All-Wheel Drive System

by

Yi Zhang

APPROVED BY:

_____

S. Das
Department of Civil and Environmental Engineering

_____

E. Lang
Department of Mechanical, Automotive & Materials Engineering

_____

L. Oriet, Advisor
Department of Mechanical, Automotive & Materials Engineering

September 15, 2017

DECLARATION OF CO-AUTHORSHIP / PREVIOUS PUBLICATION

I. Co-Authorship

I hereby declare that this thesis does not incorporate material that is result of joint research. In all cases, the key ideas, primary contributions, simulation model, data analysis and interpretation, were performed by the author, Dr. E. Lang and Dr. L. Oriet as advisor. In addition, Z. Tang provides experience knowledge throughout the research project.

I certify that, with the above qualification, this thesis, and the research to which it refers, is the product of my own work.

II. Previous Publication

This thesis reflects the content of 7 Chapters that have been previously published/submitted for publication in peer reviewed journals and conferences, as follows:

Thesis Chapter	Publication title/full citation	Publication status*
Chapter [1]	*Zhang,Y. Oriet,L. Lang,E. and Tang,Z. "The Application of Regenerative Braking System to the Commercial Hybrid Vehicles with All-Wheel Drive System", in Proceedings of the AVL International Simulation Conference 2017, Graz, AT, Jun. 2017.*	*Submitted*
Chapter [3]	Zhang,Y. Oriet,L. Lang,E. and Tang,Z. "The Application of Regenerative Braking System to the Commercial Hybrid Vehicles with All-Wheel Drive System", in Proceedings of the AVL International Simulation Conference 2017, Graz, AT, Jun. 2017.	*Submitted*

Chapter [4]	Zhang,Y. Oriet,L. Lang,E. and Tang,Z. "The Application of Regenerative Braking System to the Commercial Hybrid Vehicles with All-Wheel Drive System", in Proceedings of the AVL International Simulation Conference 2017, Graz, AT, Jun. 2017.	*Submitted*
Chapter [5]	Zhang,Y. Oriet,L. Lang,E. and Tang,Z. "The Application of Regenerative Braking System to the Commercial Hybrid Vehicles with All-Wheel Drive System", in Proceedings of the AVL International Simulation Conference 2017, Graz, AT, Jun. 2017.	*Submitted*
Chapter [6]	Zhang,Y. Oriet,L. Lang,E. and Tang,Z. "The Application of Regenerative Braking System to the Commercial Hybrid Vehicles with All-Wheel Drive System", in Proceedings of the AVL International Simulation Conference 2017, Graz, AT, Jun. 2017.	*Submitted*
Chapter [7]	Zhang,Y. Oriet,L. Lang,E. and Tang,Z. "The Application of Regenerative Braking System to the Commercial Hybrid Vehicles with All-Wheel Drive System", in Proceedings of the AVL International Simulation Conference 2017, Graz, AT, Jun. 2017.	*Submitted*
Chapter [8]	Zhang,Y. Oriet,L. Lang,E. and Tang,Z. "The Application of Regenerative Braking System to the Commercial Hybrid Vehicles with All-Wheel Drive System", in Proceedings of the AVL International Simulation Conference 2017, Graz, AT, Jun. 2017.	*Submitted*

I certify that I have obtained a written permission from the copyright owner(s) to include the above published material(s) in my thesis. I certify that the above material

describes work completed during my registration as a graduate student at the University of Windsor.

III. General

I declare that, to the best of my knowledge, my thesis does not infringe upon anyone's copyright nor violate any proprietary rights and that any ideas, techniques, quotations, or any other material from the work of other people included in my thesis, published or otherwise, are fully acknowledged in accordance with the standard referencing practices. Furthermore, to the extent that I have included copyrighted material that surpasses the bounds of fair dealing within the meaning of the Canada Copyright Act, I certify that I have obtained a written permission from the copyright owner(s) to include such material(s) in my thesis.

I declare that this is a true copy of my thesis, including any final revisions, as approved by my thesis committee and the Graduate Studies office, and that this thesis has not been submitted for a higher degree to any other University or Institution.

ABSTRACT

The growing issues of energy shortage and the environmental crisis has resulted in new challenges for the automotive industry. Conventional commercial vehicles, such as refuse trucks and delivery vehicles, consume significantly more energy than other on-road vehicles since they have the characteristic of frequent start/stop with high moment of inertia and drive at low speeds on designated city routes. It is important to make these vehicles more fuel efficient and environmentally friendly. The hybrid commercial vehicle is a promising solution to reduce emissions and to meet the future vehicle emission standard since it is generally equipped with braking energy regeneration systems to recover the kinematic loss from frequent braking. This paper introduces a type of all-wheel drive hybrid concept suggested by Dr. Leo Oriet; the new concept allows commercial vehicles to have a significant improvement in kinetic braking energy recovery without sacrificing braking safety. Without mechanical connection involved to transfer energy within the powertrain, greater powertrain efficiency can be achieved. The research is based on the all-wheel drive with a two-axles regenerative braking strategy and driveline control unit. The vehicle model and driveline control unit were executed using AVL CRUISE to demonstrate its reliable braking energy regeneration system, effective energy management and emission reduction. Finally, the power system and engine operating condition, as well as vehicle driving mode, were analyzed after simulation to ensure the whole powertrain component functions together with high efficiency and significant reliability.

DEDICATION

"Every challenging work needs self-efforts as well as guidance of elders especially those who were very close to our heart."

I dedicate my humble effort

To

My Parents

For earning an honest living for us and for supporting and encouraging me during my educational career

My Friends and Teachers

For inspiring me strive to be excellent and to believe in myself

ACKNOWLEDGEMENTS

This research application is derived from Dr. Leo Oriet's idea and configuration suggestions. The author acknowledges the academic and funding supports from Dr. Leo Oriet and Dr. Edward Lang, these are essential for this hybrid application development. The author also acknowledges that Harshit Coutinho technically assisted the project with expert simulation instruction. Finally, the author would like to thank University of Windsor for providing the computation and simulation software.

TABLE OF CONTENTS

LIST OF TABLES

LIST OF FIGURES

LIST OF APPENDICES

LIST OF ABBREVIATIONS/SYMBOLS

SOC	state of charge
SOH	state of health
ISA	integrated starter alternator
HEV	hybrid electric vehicle
EGR	exhaust gas recirculation
DPF	diesel particulate filter
CW	curb weight
GVW	gross vehicle weight
GCW	gross combination weight
UDS	urban dynamometer driving
DC	direct current
AC	alternating current
IC	internal combustion
ABS	anti-lock braking system
GHG	greenhouse gas
NOx	nitrogen oxides
RDE	real driving emission test
ESC	European stationary cycle
PEMS	portable emission measurement system
CVS	constant volume sampling

NOMENCLATURE

F_a	Aerodynamic force
F_{rr}	Rolling resistant force
F_{rr}	Gravity force
p_a	Atmospheric pressure
C_r	Rolling resistant coefficient
C_D	Aerodynamic drag coefficient
μ	Adhesive coefficient
A_f	Front area
δ	Mass factor
$p_{Y,con}$	Brake pressure
$p_{Y,b}$	Brake pressure rear axle
$p_{Y,f}$	Brake pressure front axle

CHAPTER 1

INTRODUCTION

Introduction

In recent years, because of the lack of reliable alternative energy sources, increasing efficiency and reducing exhaust gas emissions has become the focus of the modern automotive research. Commercial vehicles such as refuse trucks and delivery vehicles lose a tremendous amount of kinetic energy during frequent braking and constant drive at low speeds on designated city routes, which results in higher fuel consumption and GHG emission than other on-road vehicles [6]. Numerous attempts have been made to improve type of vehicles. The technological combination of EGR and DPF after treatment is one of the effective ways to solve the vehicle emission, especially for NOx and soot. However, this method is not able to reduce the GHG emission since the low temperature combustion of this technology results in increasing the fuel penalty. Sacrificing engine efficiency in exchange for reduced pollutants cannot fundamentally solve the energy crisis. In order to achieve overall GHG reduction targets, a strong reduction is needed particularly for commercial vehicles. As a first step, all energy should be gained from renewable sources, such as water-, sun- and wind energy. According to a statistical study done by the Canadian Electricity Association, Canada's electrical production is strongly base on hydroelectric power plant, as shown in figure (1). This energy-resource structure contributes a solid foundation for electrified commercial vehicle getting development, especially electrical vehicles and plug-in hybrids. The less fuel burnt the more GHG reduction.

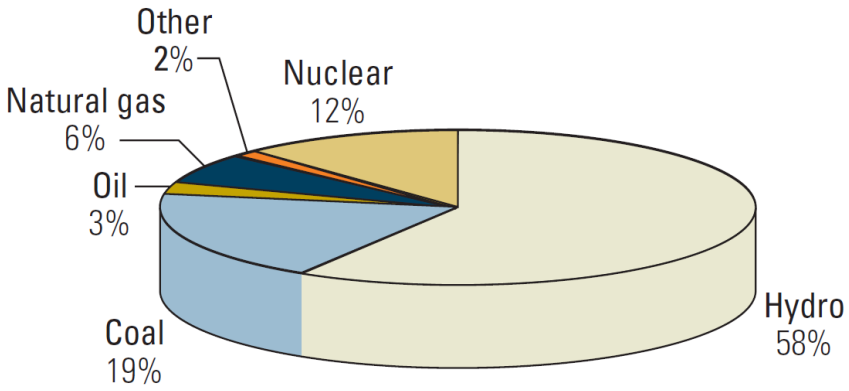

Figure 1.1 Net electricity generation in Canada, 2003[20]

Regenerative energy technology is one of the key features of electrified vehicles. It allows the vehicle to capture a tremendous amount of the kinetic energy lost during braking or decelerating for reuse. That is saying, energy recovery technology can significantly bring down the energy consumption of electrified vehicle, particularly in urban operated route. Generally, there are two regenerative energy approaches which have been applied to commercial vehicles: Regenerative Braking System and Boost Recuperation System. The former is usually applied in series hybrid architecture; the latter in the parallel architecture. The regenerative braking system is equipped in the driven axle to recuperate the braking energy loss. The boost recuperation system is parallelly coupled with the mechanical propulsion system to recuperate kinetic energy during the deceleration process. Both technologies allow commercial vehicles to have a significant improvement of reducing fuel consumption as well as emissions. However, few researchers have addressed the regenerative energy rate of hybrid commercial vehicles. The more energy the regenerative braking recuperates, the less fuel is consumed. Typical hybrid commercial vehicles are generally designed as rear drive and the regenerative braking system is equipped in rear driven axle(es) to recuperate the braking energy loss [9]. Due to the change of the center gravity in the vehicle under different load conditions, braking energy loss may vary in both front and rear

axles. Current braking research indicates that around 50%-80% of braking energy loss of commercial vehicles occurs in the front axle and the braking energy loss varies slightly under different load states [9]. Therefore, the majority of the regenerative energy potential is not taped.

Research Motivation and Objectives

For the purpose of increasing braking energy recovery rate, Dr. Leo Oriet has suggested a type of commercial vehicle with an all-wheel drive system, which has excellent performance in taping regenerative energy potential. This architecture, is equipped with four traction motors to recuperate kinetic braking energy loss of both front and rear axles instead of single axle regenerative braking; an ultracapacitor, series connected with the dynamic battery to absorb instantaneous high loads from the regenerative braking, to prevent the battery from frequents charging and discharging as well as supply the instantaneous high specific power to drive train; In addition, an ISA extender, allows commercial vehicles to achieve a long driving range with high efficiency engine operation. The all wheel hybrid drive-train provides a better possibility of inducing braking energy recovery by utilizing a four-electric motor drive system, this has become the best choice for the city operated commercial vehicle.

The primary target of the application is for light duty commercial vehicle, as showed in figure1.2, as suggested by Dr. Leo Oriet. This application could also apply to trailer trucks with pure electric propulsion system. The on-board battery can supply power to drive the vehicle for 1-1.5 hours satisfying the vehicle short range demands. With respect to the long-range demand, the ISA unit and IC engine have been equipped in the trailer configuration as a charger to extend the vehicle driving range. This plug-in trailer charger design, as showed in figure 1.3, has overcome the on-board space limitation and provide the possibility for the trailer truck to this all-wheel drive hybrid application.

This thesis mainly describes the principles and simulation process of all-wheel drive hybrid commercial vehicles and demonstrates its fuel economy improvement by regenerative braking system. First, it provides an overview of vehicle dynamics and the methodology of designing all-wheel drive powertrains. Secondly, this paper will discuss the key theory of braking characteristic in commercial vehicles and explain details of the regenerative braking control logic. Thirdly, the hybrid system and range extender control logic will be discussed. Finally, the process of all-wheel drive commercial vehicle modeling and simulation are elaborated.

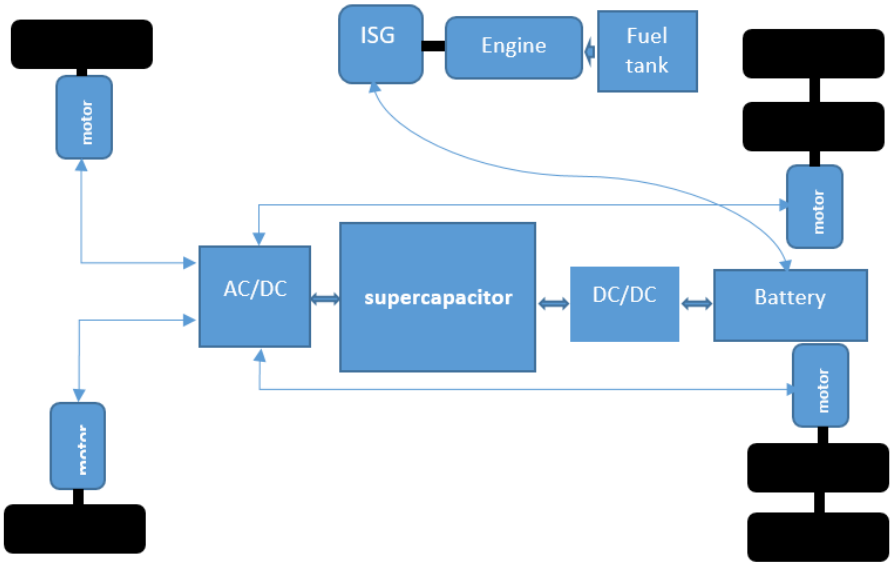

Figure 1.2 The configuration applies to medium duty commercial vehicle

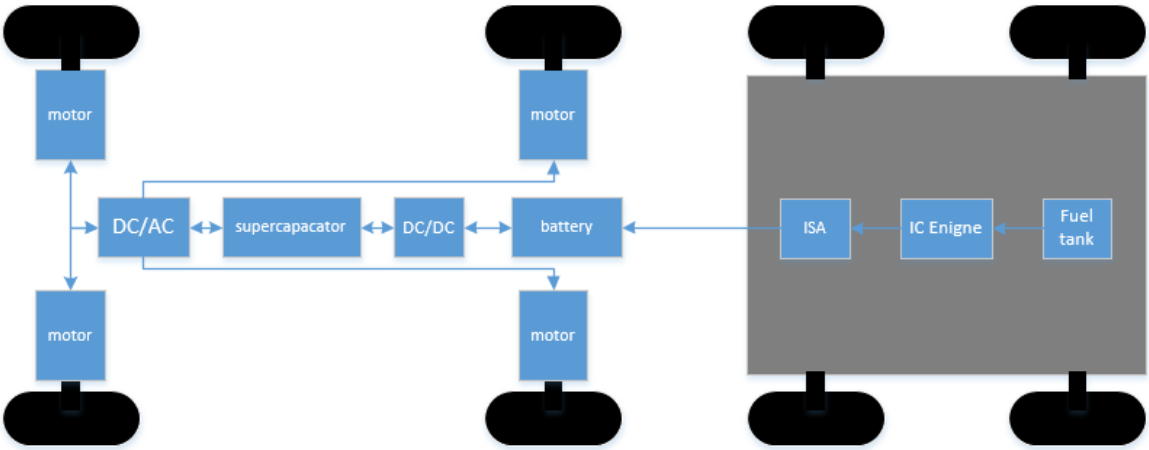

Figure 1.3 The configuration applies to trailer truck

Table 1.1 Vehicle specification

CW	7129kg	Air drag coefficient	0.52
GVW	17659 kg	Front area	$7.2\boldsymbol{m^2}$
GCW	29937kg	Front and rear axle ratio	0.461
Chassis weight (front)	2872kg	Maximum speed	105km/h
Chassis weight (rear)	2456kg	Cruising speed	83km/h
Axle Configurations	4x2 SBA	Grade capability	6%
Wheelbase	0.457 m	Rolling resistant	0.013

Methodology

This research study mainly uses the following steps to develop and manage the alternative powertrain for the all-wheel drive hybrid commercial vehicle.

Step 1: Based on vehicle dynamic constraints, calculate powertrain parameters, pre-simulate the calculation result under driving cycles, then use the pre-simulate data to propose the detail characteristics for key powertrain components. Meanwhile, collect engine, motor, as well as battery data.

Step2: Analysis the characteristics of mechanical braking and regenerative braking to propose the appropriate objectives for the development of the regenerative braking system.

Step3: On the strength of the objectives of braking system development, the actual braking curve and braking control logic will be proposed.

Step4: Model the powertrain in AVL CRUISE and program the hybrid control unit by using C code. Then the control unit will be integrated into function modules.

Step5: the model of all-wheel drive application and two comparison models are executed in AVL CRUISE. These two comparison models include a conventional truck with 16 speeds transmission and a series hybrid truck with the rear drive system. The simulation result will be analyzed with respect to braking energy and fuel consumption.

Step 6: Based on the objectives of fuel consumption and exhaust gas emission, DoE plans will be set up to further adjust powertrain parameters and to propose a better powertrain calibration plan.

CHAPTER 2

LITERATURE REVIEW

Emission Test

In order to regulate the emission of the new generation vehicle, vehicles and engines are tested for compliance with a specified vehicle driving or engine operating schedule, which consists of speed/load vs time in a government-certified laboratory. The testing schedule, or so-called driving cycle, is used to create real time vehicle driving conditions or engine operating patterns. The emission sampling devices are connected to the exhaust pipe to analyze the composition of emitting gas and provide a quantitative assessment of fuel consumption, emissions, greenhouse gases, etc. Three types of emission testing are specified in current and future standards including chassis dynamometer testing, engine dynamometer testing and on-road testing.

Chassis Dynamometer Test

For the light/medium duty vehicles and passenger cars, the testing procedure is carried out in the chassis testbed within a thermal controlled environment, as shown in Figure (5). The limits are defined in terms of mass of pollutant emitted per unit distance travelled i.e., g/km (g/mile in the USA , 1 g/km =1.61 g/mile) [22]. The testing room usually has a big underground elevator that can store four or five passage cars. The testing procedure strictly enforces vehicle thermal state; to be tested the vehicle must rest overnight in the elevator before testing by soaking in the ambient temperature and humidity. After an overnight "soak," the vehicle is placed on the testbed roller for running the following tests, including cold starts, transient driving, stops, and hot starts, as shown in Figure (4) [22].. The friction material with specific adhesion coefficient is used on the testing rotor to provide the real-time road surface. Based on the vehicle testing speed, a cooling fan located in front of the testbed supplies varied speed flow to imitate aerodynamic force and to

cool the vehicle engine. The vehicle is operated under steady tests as well as transient tests according to the required certification. Vehicle exhaust is routed to a dilution tunnel. Then the exhaust gas is diluted with the constant flow rate by mixing it with dry cool dilution air to prevent nucleation and condensation. Standard EPA method requires that the CVS System be equipped with a full flow dilution tunnel. Finally, the sample bags are subsequently analyzed to measure different types of pollutants.

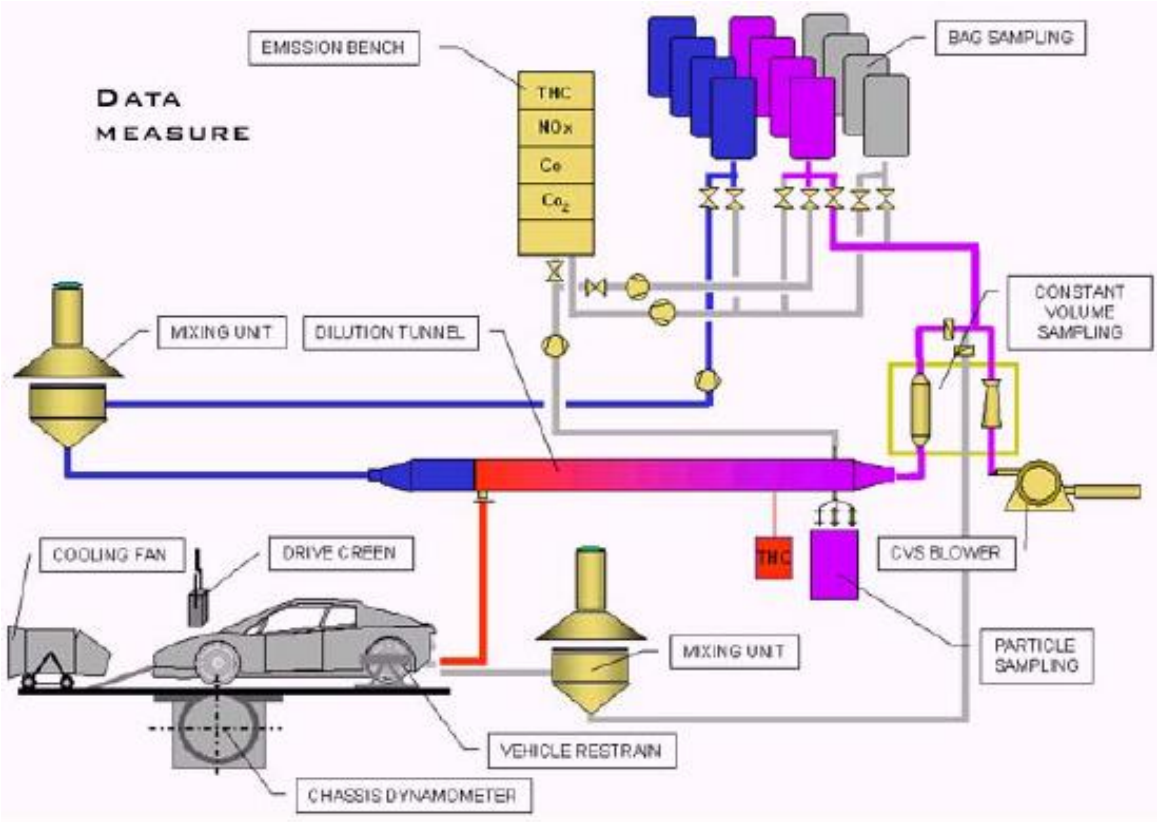

Figure 2.1 AVL chassis odynometer testbed configuration [22]

Figure 2.2 AVL chassis dynometer testbed [28]

Engine Dynamometer Test

For heavy duty vehicles and engines, that test is carried out on the engine testbed to test the engine itself, as shown in Figure2.3. The measurement standard is specified in terms of mass of pollutant per unit of work done, i.e., g/kW-h or g/bhp-h (1 g/kW-h =1.34 g/bhp-h) [22]. The R49 is one of the common certification engine test procedures. Since 2000, a new test procedure, ESC (European Steady Cycle), has replaced the R49. According to the Euro 3 standards, the test procedure consists of a 13-mode steady state cycle (ESC)with a European Load Response (ELR). From the Euro 4 standards implemented in 2005, all heavy-duty engines are tested by both the ESC and ETC (European Transient Cycle) test procedure. The ESC is performed on the engine dynamometer operated through a sequence of 13-mode (speed and load conditions). Each mode had a different weighing factor. The final test result is a weighted average of the exhaust emissions for all the 13 modes, as shown in Figure2.4 [22] [8]. ELR is performed by a sequence of three-load steps at each of the three engine speeds to measure engine smoke. The ETC has been developed by the former FIGE Institute, Aachen, Germany, based on real road cycle measurements of heavy

duty vehicles (FIGE Report 104 05 316, January 1994). The testing conditions are represented by three parts of the ETC cycle, including urban, rural and motorway driving.

Figure 2.3 AVL engine dynometer testbed [28]

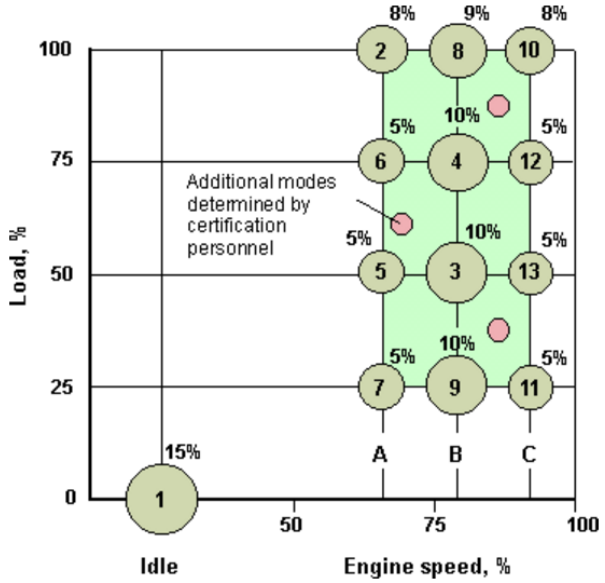

Figure 2.4 European stationary cycle (ESC) [30]

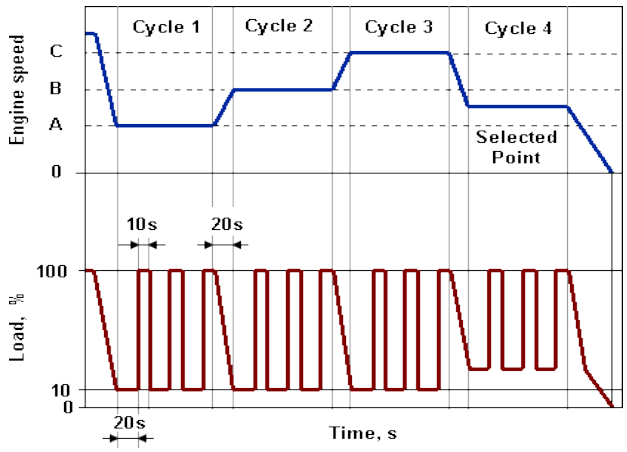

Figure 2.5 ELR Test [30]

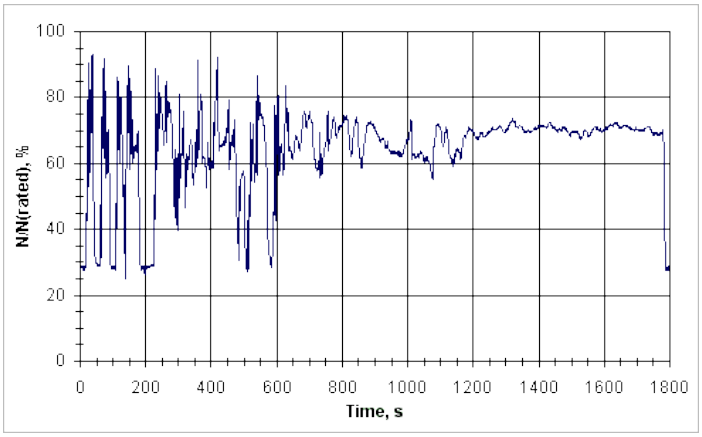

Figure 2.6 ETC Transient Cycle—Engine Speed [30]

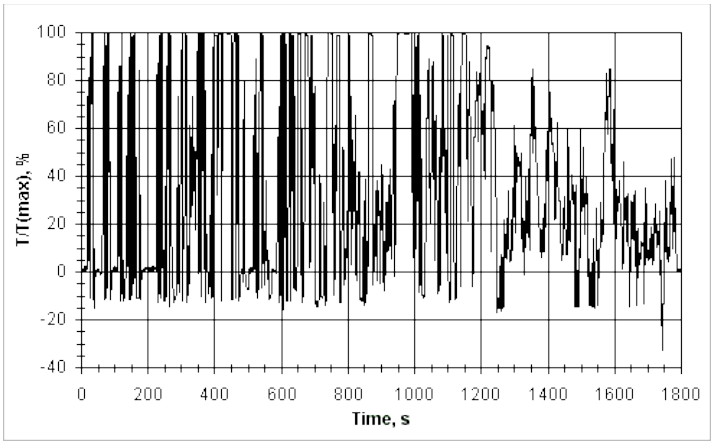

Figure 2.7 ETC Transient Cycle—Engine Torque [30]

Real Driving Emissions Test (RDE)

RDE testing procedure require the testing vehicle to be parked overnight in an unheated garage. It is conducted as a 3-days test over a fixed route, with 4 tests per day, each lasting approximately one hour. The testing vehicle is driven on real traffic roads and exposed to a wide range of different conditions[22]. The portable emissions measurement system (PEMS) is installed on the vehicle for raw, undiluted gas sampling directly from the exhaust, as shown in Figure2.8. The collected data is used to verify that legislative certification for pollutants such as NOx are not exceeded. Driving conditions include low and high altitudes; year-round temperatures; additional vehicle payload; up- and down-hill driving; urban roads (low speed); rural roads (medium speed); motorways (high speed). This Real Driving Emissions test will be implemented as an additional approval requirement in upcoming EU7 Emission Regulations.

Figure 2.8 The AVL M.O.V.E GAS PEMS is Portable Emission Measurement System (PEMS) [28]

Emission Standards

The emission standards are dedicated to gradually bringing down the level of vehicle emission pollution. These standards are established by the major Regulatory Agencies including U.S. Environmental Protection Agency (EPA); California Air Resources Board (CARB); European Economic Community (EEC); Japanese Ministry; International Convention on the Prevention of

Pollution from. Exhaust pollutants may vary significantly due to different combustion technologies. Main pollutants of gasoline can include CO, HC, and CO2 and NOx. As a result of diffusion combustion, the diesel car may emit certain PM besides CO, HC, CO2 and NOx. Although CO2 can enhance the greenhouse effect and influence climate change, it is exempt from the pollutant regulations since CO2 does not harm human health compared to other pollutants. Hydrocarbons and oxides of nitrogen can result in photochemical reactivity, which will affect human health and damage plants. The pollutant concentration and exposed duration are two leading factors that affect human health, as shown in Figure2.9.

Pollutants	Short-term health effects	Long-term health effects
Carbon monoxide	Headache, shortness of breath, dizziness, impaired judgment, lack of motor coordination	Effects on brain and central nervous system, nausea, vomiting, cardiac and pulmonary functional changes, loss of consciousness and death
Nitrogen dioxide	Soreness, coughing, chest discomfort, eye irritation	Development of cyanosis especially at lips, fingers and toes, adverse changes in cell structure of lung wall
Oxidants	Difficulty in breathing, chest tightness, eye irritation	Impaired lung function, increased susceptibility to respiratory function
Ozone	Similar to those of NO_2 but at a lower concentration	Development of emphysema, pulmonary edema
Sulfates	Increased asthma attacks	Reduced lung function when oxidants are present
TSP/Respirable suspended particulate	Increased susceptibility to other pollutants	Many constituents especially poly-organic matter are toxic and carcinogenic, contribute to silicosis, brown lung

Figure 2.9 Adverse Health Effects of vehicle exhaust[21]

US Standards

The US emission standards are different for light duty and heavy duty vehicles as shown in Figure 2.13 and Figure 2.14. the regulations were set for the first time under the Clean Air Act of 1968. Later amended standards to the Clean Air Act were further tightening emission limitations. In the

meantime, California introduced a new set of emission regulations (Figure2.12) and called the vehicles meeting these regulations by the name of different grades of low emission vehicles (LEV) such as TLEV (Transitional), LEV, ULEV (Ultra), SULEV (Super Ultra) and Partial zero emission vehicles (PZEV). According to EPA regulations, the majority of the driving cycle for light duty vehicle certification use transit testing schedule. With respect to heavy duty engine, the testing procedure consist of both steady and transit testing schedule.

Year	NMOG/ NMHC	CO	NO_x	PM (1)	HCHO(2)	Evap. g/test
US Federal						
Pre-control (1966)	15 (3)	90	6.2			6.0
1975	1.5 (3)	15	3.1			2.0 (4)
1981	0.41 (3)	3.4	1.0			2.0 (5)
Tier1(6) , 1994						(7)
Gasoline	0.25(0.31)	3.4 (4.2)	0.4 (0.6)	-		
Diesel	0.25(0.31)	3.4 (4.2)	1.0 (1.25)	0.08 (0.10)		
Tier2 (8) , 2004 - 2009	0.125	1.7	0.2	0.02	0.018	(7)

NMHC/NMOG = Non-methane hydrocarbons or organic gases

Figure 2.10 US Federal Emission Standards for light duty vehicle, g/mile [23]

Year	CO	HC	NMHC + NO_x	NO_x	PM
1988	15.5	1.3	-	10.7	0.60
1990	15.5	1.3	-	6.0	0.60
1991	15.5	1.3	-	5.0	0.25 (0.25)
1994	15.5	1.3	-	5.0	0.10 (0.07)
1996	15.5	1.3	-	5.0	0.10 (0.05) (1)
1998	15.5	1.3	-	4.0	0.10 (0.05)(1)
2004(2)					
Option 1	15.5	-	2.4	-	0.10 (0.05)
Option 2	15.5	0.5 (3)	2.5	-	0.10 (0.05)
2007	15.5	0.14 (3)	-	0.2	0.01

Note: values in parentheses apply to urban buses

Figure 2.11 US Federal Heavy Duty Engine Emission Standards, g/bhp-h, (US HD-Transient cycle) [23]

Year	NMOG/ NMHC	CO	NOx	PM (1)	HCHO (2)	Evap. g/test
TLEV, 1996	0.125 (0.156)	3.4 (4.2)	0.4 (0.6)	(0.08)	0.015 (0.018)	2.0
LEV, 2000	0.075 (0.090)	3.4 (4.2)	0.2 (0.3)	(0.08)	0.015 (0.018)	2.0
ULEV, 2001	0.04 (0.055)	1.7 (2.1)	0.2(0.3)	(0.04)	0.015 (0.018)	2.0
LEV 2, 2004	0.075(0.090	3.4 (4.2)	0.05 (0.07)	(0.01)	0.015 (0.018)	2.0
ULEV2,2004	0.040(0.055)	1.7(2.1)	0.05(0.07)	(0.01)	0.008 (0.011)	2.0
SULEV2, 2004	(0.010)	(1.0)	(0.02)	(0.01)	(0.004)	2.0
PZEV (2)	0.010	1.0	0.02	0.01	0.004	

Figure 2.12 California Emission Standards for light duty vehicle, g/mile [23]

European Standards

In 1992 EU legislation approved the steady testing schedule (NEDC) for the light-duty vehicle certification. Another common driving cycle is called Artemis driving cycle. This testing schedule is derived from a statistical project done in Europe called Artemis. This driving cycle should be considered as a transit driving cycle[23]. It consists of three different configurations, plus an additional variant: the urban cycle, the rural one, the motorway 130 km/h and the motorway 150 km/h. Artemis cycles are not used for certification of pollutants or fuel consumption. However, car manufacturers use this kind of transit schedule to assess real driving conditions and vehicle performance. In order to evaluate the emission and fuel consumption under real-world driving conditions, WLTP will become the main testing procedure to replace NEDC in upcoming Europe 7. WLTP cycle is created by the Random Cycle Generation tool base on the database created with the help of a number of European countries that collaborated and provided real-world driving measurements, as shown in Figures 2.15 and 2.16 [23]. Moreover, portable emission measurement systems (PEMS) test will be considered as an additional testing requirement for all types of mass-produced vehicles; only small volume produced vehicles can be exempted.

Description	Vehicle Type	CO	HC	NO x	HC+NO x	PM
1992 – Euro 1	All	2.72	-	-	0.97	0.14 (1)
		(3.16)			(1.13)	(0.18) (2)
1996 – Euro 2	Gasoline	2.2	-	-	0.50	-
	Diesel IDI	1.0	-	-	0.70	0.08
	Diesel DI	1.0	-	-	0.90	0.10
2000 - Euro 3 (3)	Gasoline	2.3	0.20	0.15	-	-
	Diesel	0.64	-	0.50	0.56	0.05
	Gasoline	1.00	0.10	0.08	-	-
2005 – Euro 4	Gasoline	1.00	0.10	0.08	-	-
	Diesel	0.50	-	0.25	0.30	0.025
2009 - Euro 5	Gasoline	1.0	0.10 (4)	0.06	-	0.005 (5,6)
	Diesel	0.50	-	0. 18	0.23	0.005 (6)
2014 – Euro 6	Gasoline	1.0	0.10 (4)	0.06	-	0.005 (5,6)
	0.50	-	0. 08	0.17	0.17	0.005 (6)

Figure 2.13 European emission standards for light duty vehicle, g/km[23]

	Date & Category	Test cycle	CO	HC	NO_x	PM	Smoke
Euro1	1992 <85 kW	ECE R-49	4.5	1.1	8.0	0.61	
	1992 >85 kW		4.5	1.1	8.0	0.36	
Euro 2	Oct. 1996		4.0	1.1	7.0	0.25	
	Oct. 1998		4.0	1.1	7.0	0.15	
Euro 3	Oct. 2000	ESC & ELR	2.1	0.66	5.0	0.10	0.8
						0.13*	
Euro 4	Oct 2005	ESC& ELR	1.5	0.46	3.5	0.02	0.5
Euro 5	Oct. 2008		1.5	0.46	2.0	0.02	0.5
Euro 6	Jan. 2013	ESC	1.5	0.13	0.4	0.01	-

Figure 2.14 European heavy duty diesel (CI) engine emission standards – g/kWh (smoke in m -1) [23]

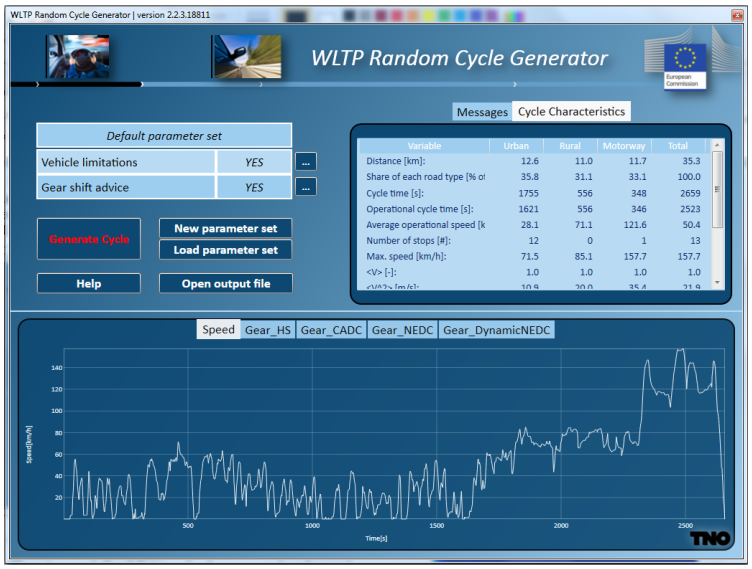

Figure 2.15 WLTP random cycle generator tool speed results[32]

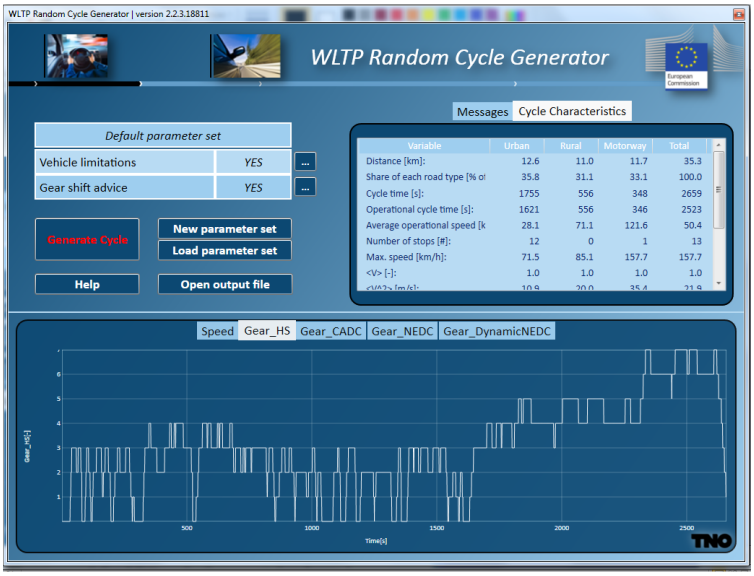

Figure 2.16 WLTP random cycle generator tool gear shift results [32]

Driving Cycles Summary

Base on emission test demand or real driving conditions, a number of driving cycles are established by emission test authorities or institutions.Table2.1, Table2.2, and Table 2.3 are the summary of the previous and current emission test driving cycles.

Table 2.1 International emission test cycles [24]

Worldwide Harmonized Light Vehicles Test Cycle (WLTC)	Chassis dynamometer test cycles for light-duty vehicles used for vehicle emission certification/type approvals conducted in the EU and other countries according to the Worldwide Harmonized Light Vehicles Test Procedures (WLTP).
World Harmonized Stationary Cycle (WHSC)	A steady-state engine dynamometer cycle for heavy-duty engines, developed for engine emission certification/type approvals worldwide.
World Harmonized Transient Cycle (WHTC)	A transient engine dynamometer cycle for heavy-duty engines, developed for engine emission certification/type approvals worldwide.
World Harmonized Vehicle Cycle (WHVC)	A non-regulatory chassis dynamometer test cycle for heavy-duty vehicles.
Nonroad Transient Cycle (NRTC)	A transient engine dynamometer cycle for mobile nonroad engines, used for engine emission certification/type approval in the USA, European Union and other countries.
ISO 8178	Test cycle composed of several steady-state test modes. Used for selected non-road engine applications in Europe, USA, and Japan.

Table 2.2 United states emission test cycles[24]

Light-Duty Vehicles	
FTP 72	A transient test cycle for cars and light duty trucks performed on a chassis dynamometer. Simulates a urban route with frequent stops.
FTP 75	A transient test cycle for cars and light duty trucks derived from the FTP-72. Used for emission certification testing of cars and light duty trucks in the USA.
SFTP US06	A supplemental FTP procedure to simulate aggressive highway driving.

SFTP SC03	A supplemental FTP procedure to simulate emissions associated with the use of air conditioning units.
New York City Cycle	EPA NYCC schedule simulating low speed city driving.
Highway Fuel Economy Test (HWFET)	EPA dynamometer driving schedule for fuel economy determination.
California Unified Cycle (UC, LA92)	California UC dynamometer driving schedule.
Standard Road Cycle (SRC) and Standard Bench Cycle (SBC)	Dynamometer and engine bench tests for emission durability determination.
Heavy-Duty Engines (Engine Dynamometer)	
FTP Transient	A transient engine dynamometer cycle for heavy-duty truck and bus engines. Includes segments designed to simulate both urban and freeway driving. Used for emission certification testing of heavy-duty diesel engines in the USA.
Supplemental Emissions Test (SET)	Supplementary steady-state test used for emission certification of heavy-duty diesel engines in the USA.
NTE (Not-To-Exceed) Testing	Additional US EPA testing requirements for emission certification of heavy-duty diesel engines.
AVL 8-Mode Heavy-Duty Cycle	A steady-state test designed by AVL to produce emission results closely correlating with those measured over the US.
CSVL	Constant-Speed, Variable-Load (CSVL) transient test cycle developed by the EPA for constant-speed engines, but never adopted in emission regulations.
Heavy-Duty Vehicles (Chassis Dynamometer)	
Urban Dynamometer Driving Schedule (UDDS)	EPA transient chassis dynamometer test cycle for heavy-duty vehicles.
Central Business District (CBD)	Transient chassis dynamometer test cycle for heavy-duty vehicles.
Business Arterial Commuter (BAC)	A composite heavy-duty vehicle's fuel economy cycle, also known as the Transit Coach Operating Duty Cycle.
City Suburban Cycle & Route (CSC)	Chassis dynamometer test cycle for heavy-duty vehicles.

Neighborhood Refuse Truck Cycle	Transient chassis dynamometer test cycle representing the operation of a refuse truck.
New York Bus (NYBus)	Transient chassis dynamometer test cycle for urban transit buses.
Heavy Heavy-Duty Diesel Truck (HHDDT)	Four-mode chassis dynamometer test developed by the California Air Resources Board.

Table 2.3 European union emission test cycles [24]

Light-Duty Vehicles	
ECE+EUDC / NEDC	A combined chassis dynamometer test used for emission testing and certification in Europe. It is composed of four ECE Urban Driving Cycles, simulating city driving, and one Extra Urban Driving Cycle (EUDC), simulating highway driving conditions. The cold-start version of the test, introduced in 2000, is referred to as the New European Driving Cycle (NEDC).
Common Artemis Driving Cycles (CADC)	Chassis dynamometer test cycles (urban, rural road and motorway) developed under the Artemis project, based on statistical analysis of European real world driving conditions.
ADAC Highway Cycle (BAB 130)	Chassis dynamometer test cycle representing high speed highway driving used for ADAC EcoTest testing.
RTS 95 Cycle	Chassis dynamometer test cycle representing aggressive driving.
Heavy-Duty Engines & Vehicles	
ECE R49	Steady state cycle for heavy duty truck engines. Consists of a sequence of 13 engine dynamometer test modes. Used for heavy-duty engine emission certification through the Euro II stage.
ESC (OICA)	Steady-state cycle for truck and bus engines. The ESC test is used for emission certification of heavy-duty diesel engines from the Euro III stage (2000).
ELR	Test is used for smoke opacity determination during emission certification of heavy-duty diesel engines from the Euro III stage (2000).
ETC (FIGE)	Transient test cycle for truck and bus engines. It is used, together with the ESC, for heavy duty engine emission certification. A non-

	standardized vehicle version, known as FIGE cycle, is sometimes used for research purposes.
Braunschweig Cycle	Transient chassis dynamometer test cycle simulating a urban bus route.

Model based development and calibration

Model based development and calibration are implemented in many types of industries and bring significant benefits, including increased accuracy and complexity of powertrain design, a reduction of development and calibration costs, and shortened development and testing time. Powertrain and engine development also use this procedure. As is shown in the V model, before the prototype undergoes the approval test, the early stage concept of the powertrain should go through a model in the loop test (MIL), hardware in the loop test, testbed measuring, and road testing, as it shown in figure2.17.

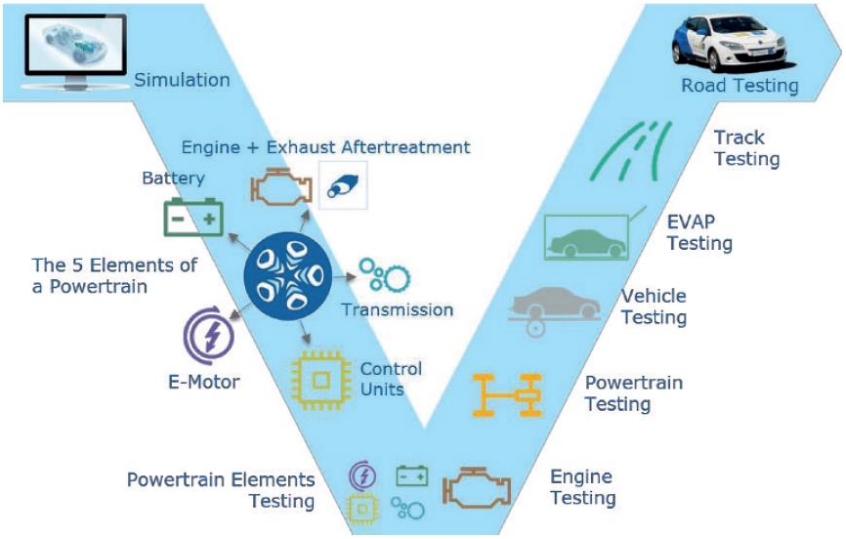

Figure 2.17 V model of AVL powertrain development [34]

AVL CRUISE is one of the most common used MIL testing software in automotive industry. The powertrain model of AVL cruise consist of both an empirical model and physical components. The empirical model components of the powertrain are derived from either AVL testbed data or one's

own experimental data, and the physical components are defined in the user guide. Each module of the model describes the specifications, operation, and performance of specific components. All the powertrain components are integrated together, either by a mechanical connection, or by an electrical connection, at which point they form a large system. MIL testing is used throughout development stages, including Research, Design, Implementation, Evolution, and Verification. At each stage of development, the model is updated and refined to increase simulation accuracy. MIL test is carried out on the virtual hardware device and the real ECU controller. Basically, the physical plant of MIL has been download into virtual hardware, such as dspace and ETAS. Meanwhile, the ECU of the model is converted into C code and then embedded into a real controller. Finally, the HIL test can be operated after data bus connection. The accuracy of the HIL test is highly depended on the complexity of physical model. It may have more accuracy than MIL since the hardware can imitate injection delay, battery aging, and other functions. The HIL is used in many development and calibration areas, such as ECU, RDE, EAS, and OBD [34]. Moreover, dangerous driving conditions, such as heavy rains and extreme ambient temperature, which cannot be executed in testbed, can be more ideally simulated in the HIL test. MIL and HIL tests are actually used to simulate the real testbed measurement. Parallel simulation is always necessary throughout the development process. If the simulation result has a high accuracy, MIL and HIL are recommended to replace testbed measurement in the easily development stage. As it shown in figure 2.18 and 2.19, the simulation result of AVL CRUISE generally has a lower rate deviation than the testbed measurement. This is the primary reason this software was selected to model the early concept of our hybrid application.

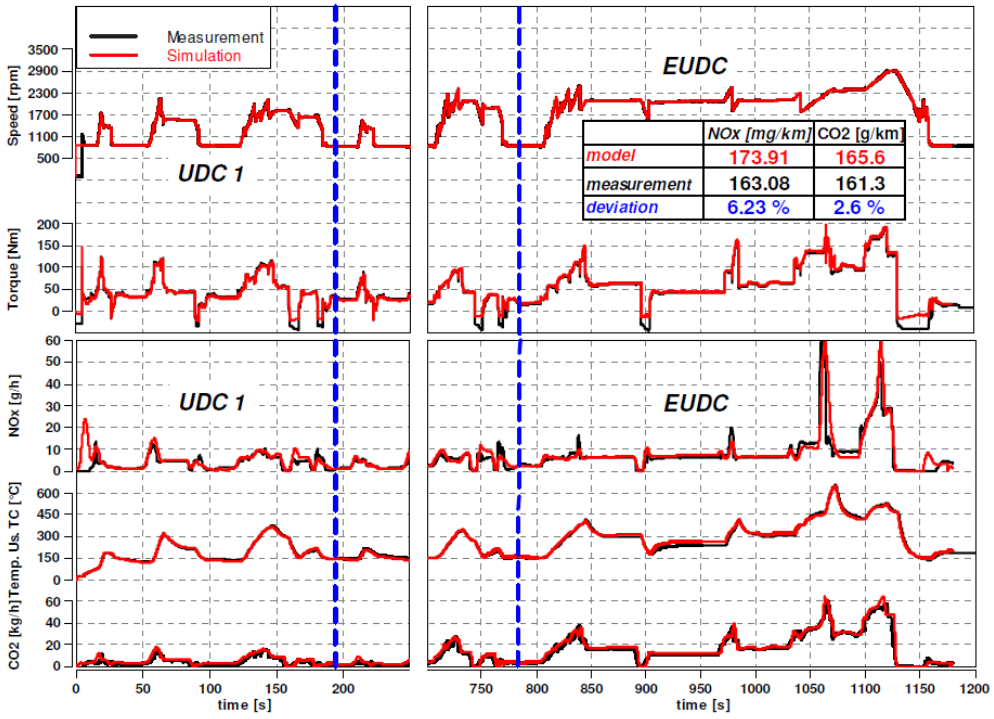

Figure 2.18 High accuracy model in NEDC test for AVL model based calibration[34]

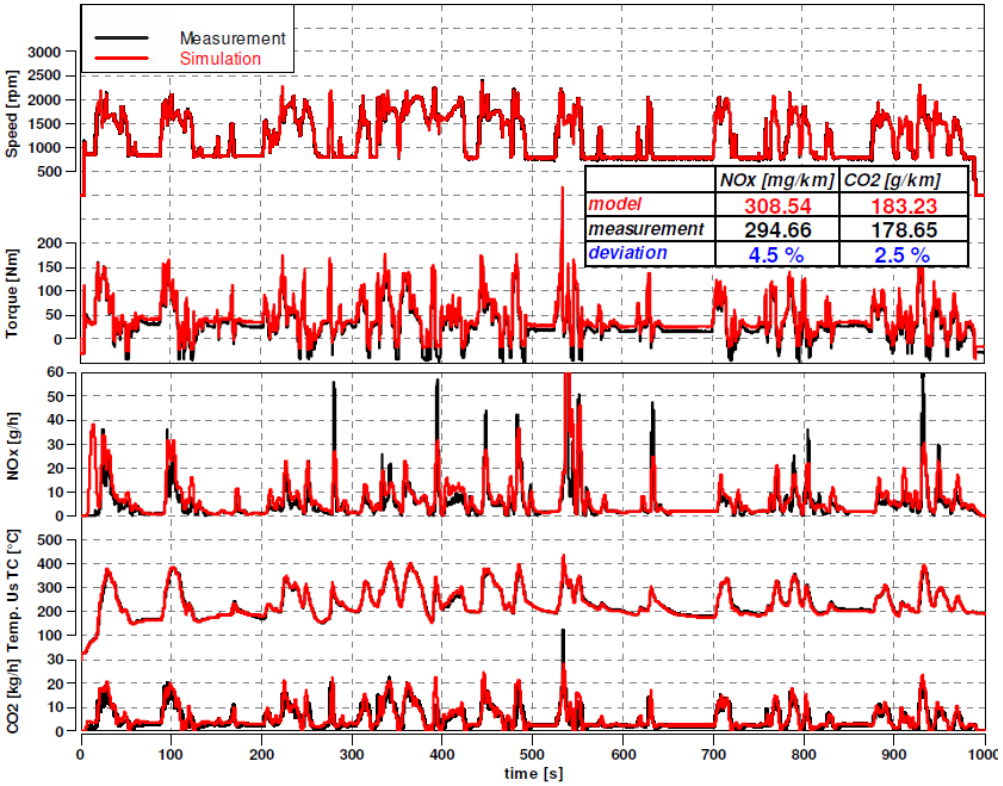

Figure 2.19 High accuracy model in Artemis test for AVL model based calibration [34]

CHAPTER 3

VEHICLE DYNAMIC

Vehicle Dynamic

According to Newton's second law, the longitudinal vehicle dynamic equation of motion is obtaining by superimposing aerodynamic drag force, rolling resistance force, gravitational force, and the inertial forces [3]. The tractive power is calculated by multiplying vehicle longitudinal velocity and tractive force [3]. In order to supply sufficient power to the vehicle, the tractive power design should be based on three factors: maximum speed capacity, grade ability, and acceleration capacity. The tractive power programs are executed by setting up the vehicle speed of the driving cycle data, according to formulas (1)(2)(3).

$$\sum F = M \cdot \text{a} \tag{1}$$

$$F_t = F_a + F_{rr} + F_g + m\delta\frac{dv}{dt} \tag{2}$$

$$P_t = VF_t = V * \left(\frac{1}{2}p_a C_D A_f V^2 + C_r mgcos\alpha + mgsin\alpha + m\delta\frac{dv}{dt}\right) \tag{3}$$

$$= \frac{1}{2}p_a C_D A_f V^3 + C_r mgVcos\alpha + mgsin\alpha + m\delta V\frac{dV}{dt}$$

```
>> fori=2:1370
Pt=0.5rho*Af*Cd(v1(i-1)^3)+m*g*v1(i-1)*cos(theta)fr+m*g*sin(theta)+v1(i-1)m(v1-v1(i-1)*del;
Tm(i)Pt;
end
```

Figure 3.1 Vehicle power calculation MATLAB program

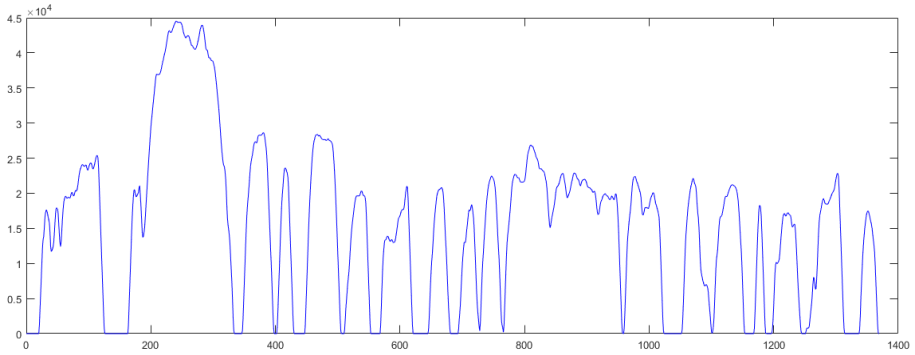

Figure 3.2 Vehicle power simulated on UDS

When the vehicle is going uphill, the gravitational force decelerates the vehicle. For downhill condition, the gravitational force accelerates the vehicle. In order to maintain constant speed, the traction force has to be adjusted positive or negative (braking), respectively [4], as shown in Figure 3.3. By assuming zero acceleration, a quadratic polynomial formula on V has been obtained with positive coefficient. According to calculation by formula (4), a1=0.45, a2= 4798 and -3427 under uphill and downhill conditions respectively.

$$F_{tr} = F_a + F_g + F_{rr}$$

$$= \frac{1}{2} p_a C_D A_f V^2 + C_r mg\cos\alpha + mg\sin\alpha + m\delta \frac{dv}{dt}$$

$$= a_1 V^2 + a_2$$

$$= 0.45V^2 + 4798(uphill)$$

$$= 0.45V^2 - 3427(downhill) \quad (4)$$

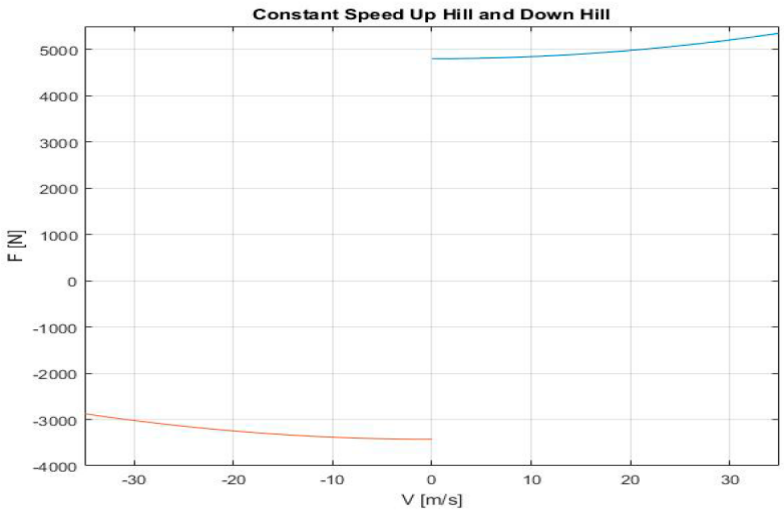

Figure 3.3 Constant speed uphill and downhill

The maximum speed of the vehicle can be obtaining by assume that the vehicle drives on horizontal road. This can estimate by formula (5) [7].

$$F_t = F_a + F_{rr} + m\delta\frac{dV}{dt} \quad (5)$$

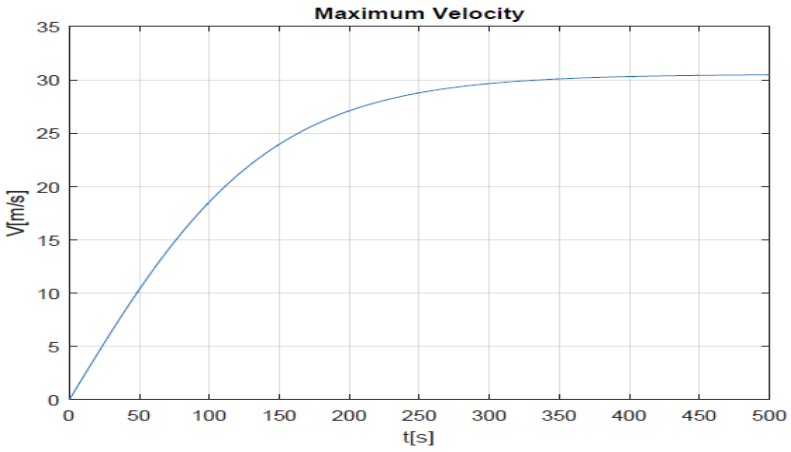

Figure 3.4 Maximum velocity

Estimation Fuel Consumption of the Typical Drivelines

Fuel consumption of the commercial vehicle have a significant effect on GHG emission. A higher GHG emission can result in more environmental pollution [8]. Based on current research, the

energy consumption of the fuel tank can be estimated by the wheel energy consumption divided by the driveline efficiency, as it shown in fomula(6). The driveline efficiency can be estimated by multiplying all component efficiencies [10]. As the calculation indicates the efficiency of all-wheel drive hybrid vehicle has a certain higher efficiency than typical series hybrid powertrain since there is no mechanical connection involved in the driveline for transferring the energy. Due to the fact that the energy is converted twice in hybrid vehicles, the powertrain efficiency of hybrid vehicle is lower than conventional powertrain. However, regenerative energy technology equipped in hybrid vehicle can allows the vehicle to recapture a tremendous amount of the kinetic energy lost for reuse during braking or decelerating. That is saying, regenerative energy technology allows hybrid powertrains in commercial vehicles to use less fuel consumption and emit less emissions.

$$E_{tank} = \frac{E_{wheel}}{\eta_{driveline}} \tag{6}$$

$$\eta_{conventional\ vehicle} = \eta_{engine} \cdot \eta_{cluth} \cdot \eta_{gear\ box} \cdot \eta_{final\ drive} \cdot \eta_{differential} \cdot \eta_{axles} = 35\% \tag{7}$$

$$\eta_{SHEV} = \eta_{engine}.\eta_{ISA} \cdot \eta_{battery} \cdot \eta_{edrive} \cdot \eta_{signle\ ratio\ gear\ box} \cdot \eta_{differential} \cdot \eta_{axles} = 25\% \tag{8}$$

$$\eta_{all-wheel\ drive\ hybrid\ vehicle} = \eta_{engine} \cdot \eta_{ISA} \cdot \eta_{battery} \cdot \eta_{DCDC} \cdot \eta_{ultracapacitor} \cdot \eta_{edrive} = 30\% \tag{9}$$

Wheel energy consumption is an approach used to estimate vehicle fuel consumption. It can be estimated by multiplying the average traction force and the unit distance (1km). The regenerative braking rate $R_{regenerative\ braking}$ plays a significant role in reducing the energy consumption of the inertia part. According to the formula (10), the more the vehicle's mass, the more the percentage reduction of wheel energy consumption can be achieved. If assuming 20% of wheel energy consumption has been recovered by regenerative braking system and the vehicle drives on horizontal ground, then according to the research data [4], 1kg of burned hydrocarbon fuel

produces around 3.5 kg of CO2 and its low heat value is about 43MJ/kg. As the carbon balance method calculation indicates, a typical series hybrid powertrain and an all-wheel drive hybrid powertrain have 16% and 19.5% less GHG emission respectively depends on location. Therefore, the characteristic of the all-wheel drive architecture provides great potential with reducing GHG emission.

$$E_{wheel} = F_{traction} \cdot d_{unit\ distence} = \left(\frac{1}{2} p_a C_D A_f V^2 + C_r mgcos\alpha + \left(1 - R_{\ regenerative\ braking}\right) m\delta \frac{dV}{dt}\right) \cdot d_{unit\ distence} \quad (10)$$

CHAPTER 4

BRAKING ANALYSIS

Regenerative Braking

Regenerative braking is one of the most important features of hybrid vehicles. During braking, the motor can function as a generator to recover the vehicle's kinetic energy and convert it into electrical energy, which can then be stored in batteries. Meanwhile, the motor will be controlled and will provide sufficient torque for braking [1].

Brakes are also a critical factor that affects vehicle safety. A well-designed braking system must provide sufficient torque to bring a vehicle to rest in the shortest distance. At the same time, it must guarantee that the rear wheels of a vehicle should not lock before the front wheels. Failing to satisfy these two demands may result in safety issues [1].

In the case of braking design, it would be possible to consider the braking force F_f and and F_r as negative since the slip-or stick friction has been ignored in longitudinal simulation [32]. In order to prevent the rear wheels from becoming locked before the front wheels, resulting in unstable braking, the actual braking force on the front wheels is usually greater than the braking force on the rear wheels. Therefore, the front and rear braking force distribution should base on the study of the ideal braking curve, as in shown in figure 4.1. The actual braking force distribution can approximately consider as a linear relationship on two braking axles.

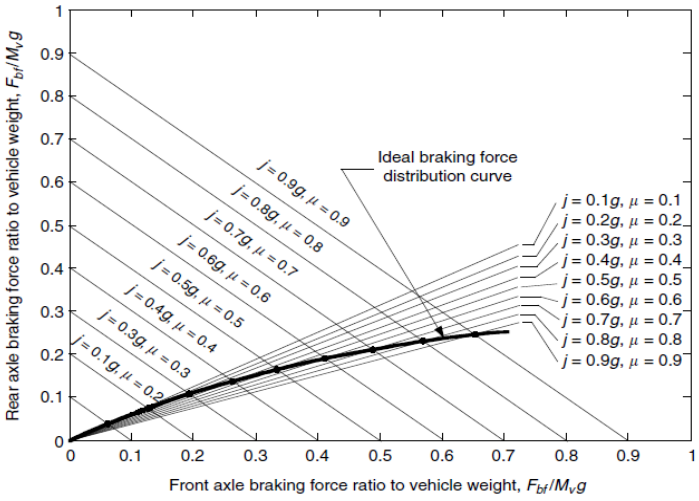

Figure 4.1 Ideal braking force distribution curve on the front and rear axles [1]

Generally, there are two type of brake control strategies: series braking and parallel braking. For the parallel braking, the conventional mechanical brake supplies a fixed ratio of braking force to the front and rear axles, as shown in Figure4.2. Regenerative braking is controlled to supply additional braking force to satisfy the total braking force distribution. This braking strategy sets up a limit for improving regenerative braking efficiency since the brake strategy relies more on mechanical brake [1].

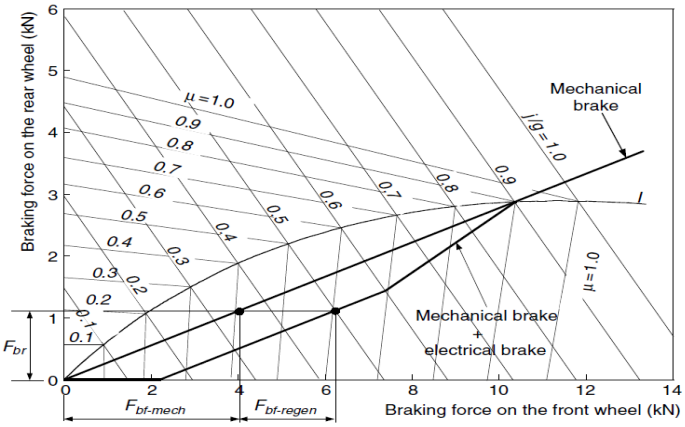

Figure 4.2 Parallel braking strategy [1]

In contrast, series braking has been use in our commercial vehicle application. Series braking is more reliant on electric regenerative braking, as shown in Figure4.3. If the demanded braking force is less than the maximum torque of the motor, only regenerative braking supplies braking force. If the commanded braking force is greater than the maximum force that the motor can produce, the mechanical brake will supply brake efforts after a fixed ratio of the braking deceleration signal [1]. Series brake has the potential to significantly improve braking energy recovery rate and provides flexibility to adjust the hybridization degree of the coexisting brakes.

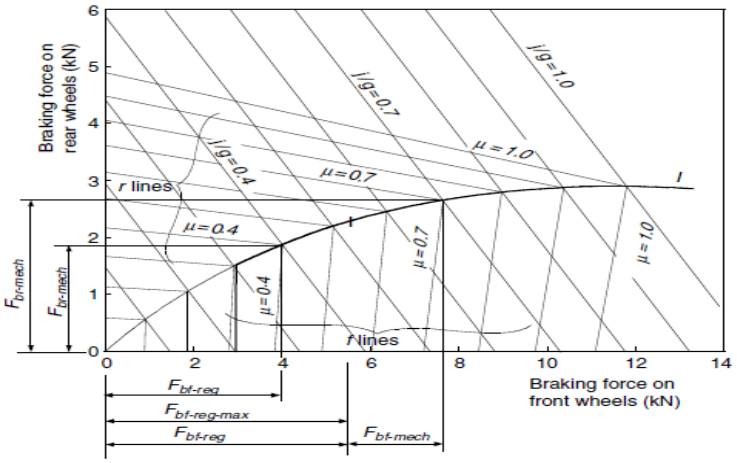

Figure 4.3 Series braking strategy [1]

One of the most interesting braking characteristic is that the braking force remains nearly constant at the speed range of less than 40km/h and decreases after speeds greater [1], as shown in Figure4.4. This characteristic naturally matches the traction motor feature that has a constant torque at the low-speed region and a constant power at the high-speed region [1]. Therefore, when designing traction motors, the braking power at 40km/h must be consider as a factor to propose the corresponding knee point of electric motor [4]. That is, if both the maximum force and power of the electric motor is no less than that of the demanded braking at the speed 40km/h, the regenerative braking can reach its highest efficiency.

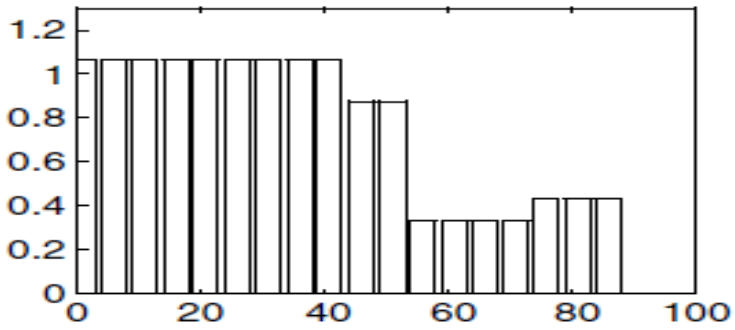

Figure 4.4 Braking torque [1]

With respect to the medium duty single rear axle commercial vehicle, the majority part of braking energy loss occurs at the low speed range, from 10 to 40 km/h. 60% of braking energy loss occurred in front axle.

Due to the large mass of commercial vehicles, the braking torque of the commercial vehicle required is much larger than the torque the electric motor can supply, so the safe braking and the recovering of kinetic energy may be in conflict situation, when there is only one traction motor in the drive train [4]. On one hand, if vehicle braking only relies on rear axles regenerative braking, though it can increase regenerative energy, the vehicle's braking distance will greatly increase since the electric motor cannot supply the large amount of braking torque the vehicle requires; this may result in braking safety issues. On the other hand, if the front axles mechanical braking coexists with the rear axle regenerative braking, it is difficult to control braking forces distribution at all vehicle axles. The unbalance braking force will affect vehicle driving direction [1]. The current hybrid commercial vehicle brake system uses mechanical brakes for the front axle and the regenerative brake for the rear axle. Such a design undoubtedly has a certain reduction for powertrain manufacture cost. However, the major part of braking energy potential hasn't been recuperated. Some solutions try to use a high-power motor only for rear axle regenerative braking

during vehicle braking. Based on current research [5], this may put braking safety and energy recovery in conflict situation.

Machinal Brakes Assembly

In order to supply deceleration, mechanical brakes have to convert the kinetic energy into heat energy, which is carried away by the air. Based on its braking method, the brakes can be classified as three types: disc brakes, drum brakes, and retarder. Disc brakes and drum brakes are generally implemented in passenger cars and light duty vehicles, as shown in Figure4.5 and 4.6 respectively. If it is classified by the transmitter, it has hydraulic brakes and air brakes. Hydraulic brakes are implemented in passenger cars, and air brakes are used for commercial vehicles since compressed air can achieve a certain higher braking pressure than a hydraulic transmitter can. The retarder is used for heavy-duty vehicles. It is equipped between gear box and propeller to slow the speed of vehicles. Two types of retarder are used on current heavy duty vehicle. Electric retarders provide a retardation force by electromagnetic induction. With respect to hydraulic retarders, the viscous drag forces between dynamic and static vanes in a fluid-filled chamber is used to supply a retardation force.

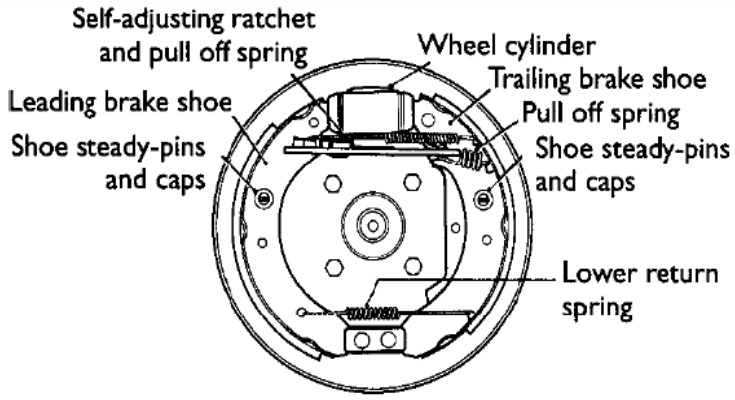

Figure 4.5 The configuration of drum brakes [32]

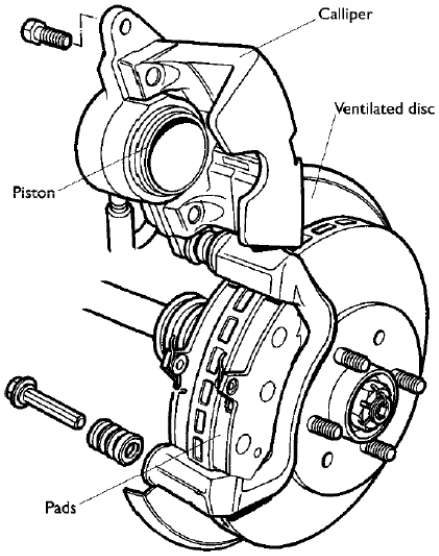

Figure 4.6 The configuration of disc brakes [32]

This chapter mainly discusses and analyses the proper way for disc brake assembly to reduce high load impact force on driven axles during vehicle braking and cornering. Disc brakes basically consist of ventilated discs, calipers, pistons, and two friction pads. Current research indicates that the assembly position has a certain influence on the driven axles' durability. Two comparison example are included to demonstrate this principle. Figure 4.7 illustrates how the braking caliper is installed at the 9 o'clock position. During braking, the force of bearing vehicle weight and the inertial force of vehicle deceleration are applied on the drive axle, indicated by green and red arrows respectively. These two forces apply on the driven axle and then form a joint force, indicated by a yellow arrow. The braking pad also supplies a friction force along the tangential line of the braking disc towards vertical direction, indicated by a blue arrow. Then, the blue arrow and yellow arrow form a new joint force, indicated by a purple arrow. Based on the force analysis, the length of the purple arrow is greater than the length of the yellow arrow. If the braking caliper is installed at around the 4:30 position, the friction force will be in the reverse direction of yellow arrow. As a result, the length of the purple arrow is shorter than the

length of the yellow arrow. Due to the optimal install position of the braking caliper, the part of impact force on the driven axle can be cancelled.

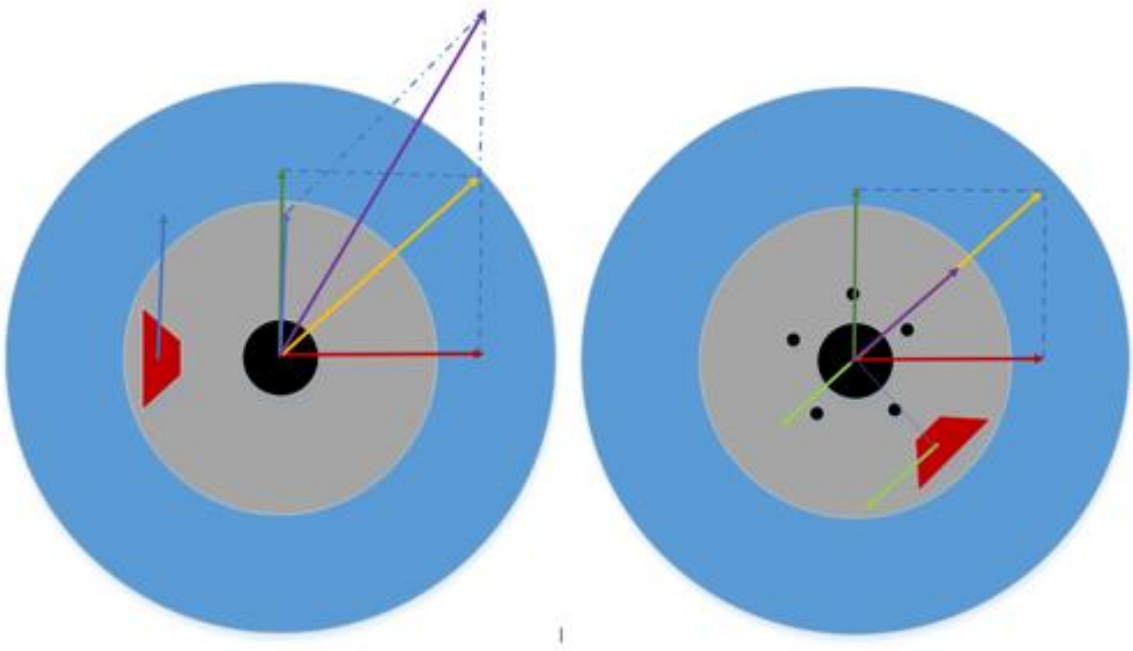

Figure 4.7 Force analysis of the vehicle tire

With respect to the braking disc assembly, the centerline of the braking disc is supposed to coincide the centerline of the tire. The red and green arrows indicate the bearing force of the vehicle weight and friction force of the brakes respectively. Failing to do this may result in a rotary torque, which impacts the top of the braking disc, causing it to wear faster. During vehicle cornering, as an impact of the centrifugal force, the outside ties bears more vehicle weight than the inside ties. The green and red arrow indicate the bearing force of the vehicle weight and the yaw force of vehicle cornering. As it shown in figure4.8, the centerline of the bearing is supposed to deviate from the centerline of tire to create a rotary torque in reverse direction to the cancelled part of the yaw force.

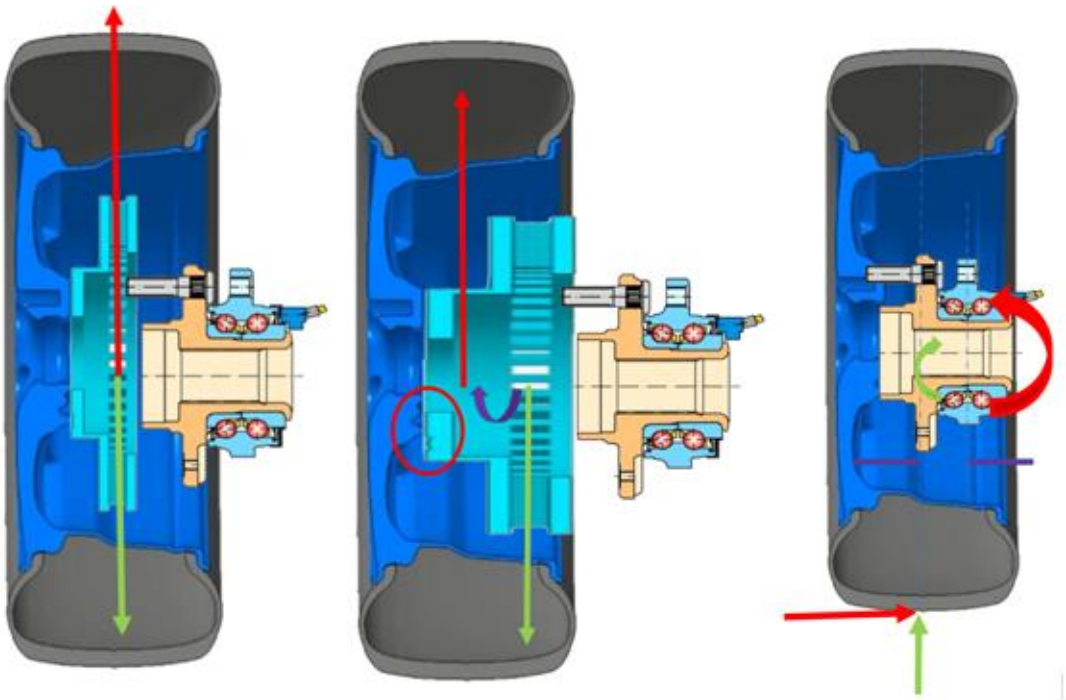

Figure 4.8 Force analysis of brakes assembly

Antilock Braking System(ABS)

Anti-lock braking system (ABS) is a braking safety system that prevents the wheels from locking up and helps avoid uncontrolled slide. It mainly consists of Tooth Wheel, Wheel Speed Sensor; ECU, and Modulator Valve, as it shown in figure4.9. Each wheel speed sensor keeps sending AC voltage signals to the ECU. Based on the frequency of the signal, the ECU continuously monitors the speed of each wheel [26].

When the vehicle is braking, all the wheels begin to slow down. ECU is programmed to identify that any of the decelerating wheels are approaching lockup [26]. If the braking force of the wheels is greater adhesive force or hard brake application or the vehicle slide occurs on a slippery surface, once such hazard braking condition occurs, ECU will adjust fluid pressure supplied to the brake chambers or control torque signal sent to the motor in an effort to prevent wheel from being locked completely.

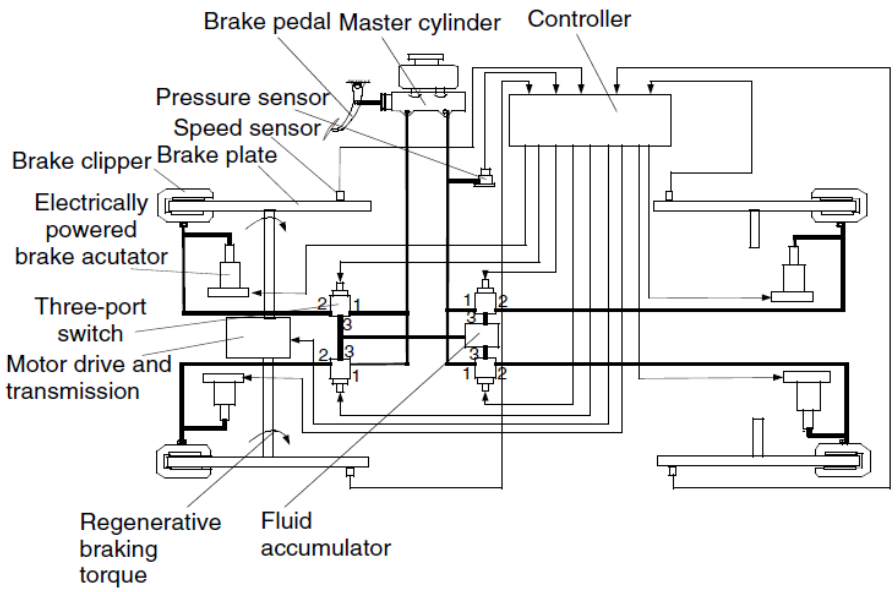

Figure 4.9 Electronically controlled anti-lock braking system configuration [1].

CHAPTER 5

THE DEVELOPMENT OF REGENERATIVE BRAKING SYSTEM

The Development of Braking Curve

When the vehicle is braking, the longitudinal tire force will be equipped to braking force if no tire slip occurs. Once the longitudinal tire force reaches the adhesive force limit, it will not follow the braking force lift but equal to adhesive force. That is saying the tire slide occurs when the braking force equal or greater than the adhesive force. The adhesive force, longitudinal tire force, and braking force can be calculated by formulas (11) (12) and (13) respectively.

$$F_{\text{adhesive force}} = \mu \cdot N \tag{11}$$

$$F_{\text{longitudinal tire force}} = m \cdot a \tag{12}$$

$$F_{\text{braking force}} = \frac{4 \cdot p \cdot A \cdot \mu \cdot R_e}{R_r} \tag{13}$$

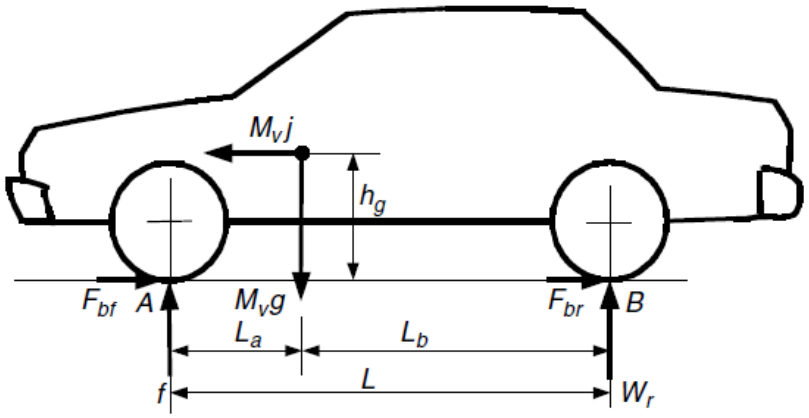

Figure 5.1 Force acting on a vehicle during braking on a flat road [1]

Due to the effect of the vehicle inertia, the center gravity of the vehicle will move forward when the vehicle decelerate, the weight bearing on the front tires increases and the weight bearing on the rear tires decreases, according to formulas (14) and (15).

$$F_{bf} = \frac{mg \cdot L_b}{(L_a + L_b)} + \frac{ma \cdot h_g}{(L_a + L_b)} \tag{14}$$

$$F_{br} = \frac{mg \cdot L_a}{(L_a + L_b)} - \frac{ma \cdot h_g}{(L_a + L_b)} \quad (15)$$

The adhesive force can be calculated by multiplying the adhesive coefficient and the support force of the tire.

$$F_{af} = \mu \cdot F_{bf} \quad (16)$$

$$F_{ar} = \mu \cdot F_{br} \quad (17)$$

$$F_{af} = m(gL_b + \mu g h_g) \cdot \mu / (L_a + L_b) \quad (18)$$

$$F_{ar} = m(gL_b - \mu g h_g) \cdot \mu / (L_a + L_b) \quad (19)$$

The ideal braking curve can be obtained from plotting the front and rear adhesive forces under varying adhesive coefficient, based on the formula (18) and (19).As it shown in figure (37), the red curve indicates the ideal braking curve under empty load state, Due to the increasing load conditions of the vehicle, braking forces distribution changes dramatically. The blue curve indicates the ideal braking curve under full load state. The actual braking curve, which indicate in green line, is the most essential data for vehicle braking strategy design. The ideal braking curve indicate that the front and rear axles lock at same time under certain braking forces distribution. However, it is challenging for actual braking curve to satisfy locking front and rear tires simultaneously since the gravity center of vehicle changes under vary load conditions. Therefore, a well-designed actual braking curve is designed to adjust the front and rear braking force to meet the reachable adhesive force as much as possible under both full load states and empty load states. To meet this design expectation, the intersection of the green line and red curve should fit into the section of $\mu(0.4 - 0.6)$; the intersection of the green line and blue curve should locate within the section of $\mu(0.7 - 1.0)$. Meanwhile, the maximum braking force should be slightly greater than the maximum adhesive force under full load state. This actual braking curve design method is derived from the experience of conventional braking system development. The braking distance and safety level are guaranteed.

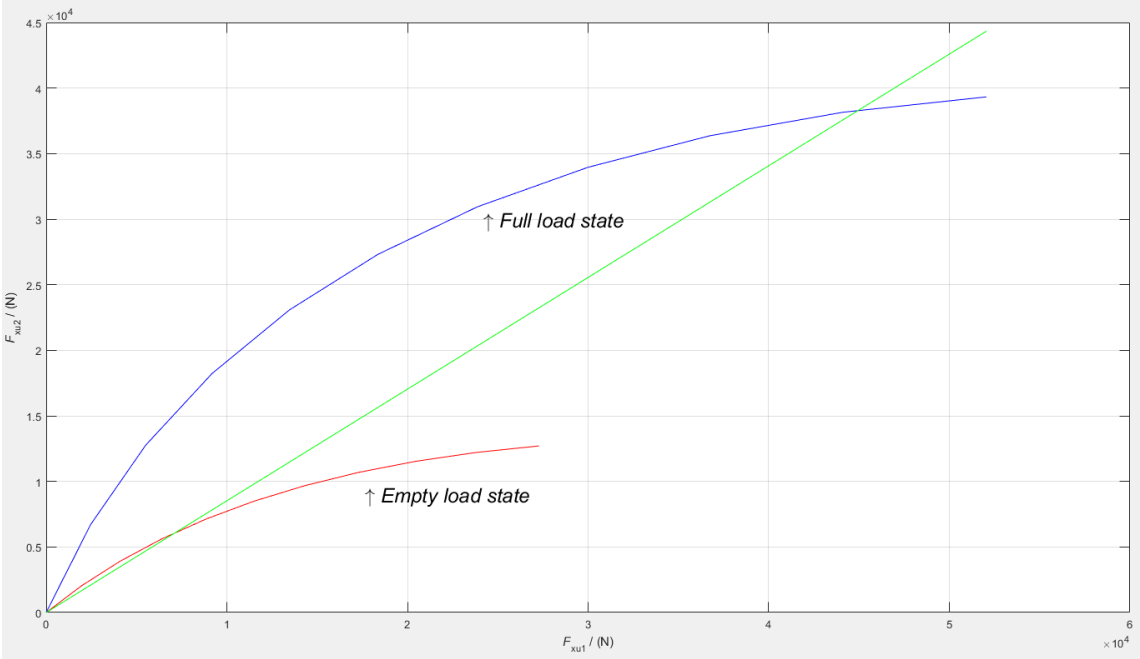

Figure 5.2 Braking curves

The Development of Braking Control Strategy

Series-braking-optimal-feel control strategy has been developed to implement this proposed actual braking curve in this research study. As indicated in Chapter 1, the proposed all-wheel-drive application is dedicated to improving the braking energy recovery rate without sacrificing braking safety. In order to improve the braking energy recovery rate, the regenerative braking must function as primary brakes at both front and rear axles. The braking strategy is elaborate in Figure5.5. The control logic consists of a two-layered control unit. Based on the actual braking curve, the first layer of the braking control unit regulates the front and rear axles' braking pressure distribution and maximum total braking force. The second layer of the braking control unit is primarily responsible for the active control of electric braking and mechanical braking forces. When the driver steps on the brake pedal, the cockpit will first receive the deceleration load signal and convert it into brake pressure. In order to achieve a better braking feeling, the braking forces of the front and rear axles should be distributed by following the actual braking curve [1]. The

demanded pressure signal will then be sent to the brake control module for redistribution. The fixed ratio of pressure reduction at the rear axle is simultaneously adjusted in this control unit, which is illustrated in Figures5.3 and 5.4:

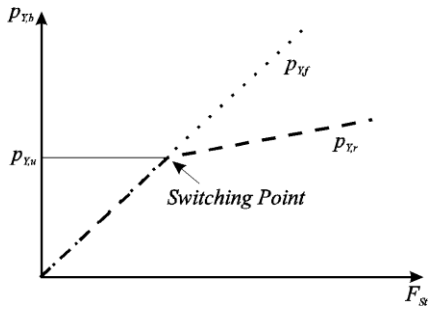

Figure 5.3 Braking pressure reduction on the rear axle [15]

After the brake pressure signal is sent to the brake control unit, the output of the front brake pressure is equal to the general brake pressure and the output of rear brake pressure has a fixed ratio reduction so as to match the ideal braking curve. As this paper illustrates in the Regenerative Braking Analysis section, the brake forces of front and rear axles can be approximated as a linear relationship.

The output brake pressure at the front axle:

$$p_{Y,f} = p_{B,com} \tag{20}$$

The output brake pressure at the rear axle:

$$p_{Y,r} = \begin{cases} p_{Y,f} & p_{Y,r} \leq p_{Y,u} \\ p_{Y,u} + \left(p_{Y,f} - p_{Y,u}\right) \cdot i_Y & p_{Y,r} > p_{Y,u} \end{cases} \tag{21}$$

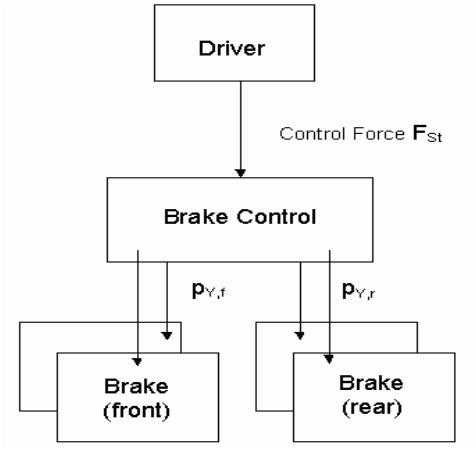

Figure 5.4 Principle representation of the brake control unit [15]

After this is processed by the brake control unit, the demanded pressure signals of front and rear axles will be sent to the two-independent regenerative braking control unit are program by C code in function modules. The two-independent regenerative braking control units which are in charge of the combination of mechanical braking and electrical regenerative braking control braking forces at front and rear axles respectively. Once the braking pressure has been sent to this module, the demanded braking force will first be calculated by using the formula (22) [13].

$$M_B = 2 \cdot p_B \cdot A_B \cdot \eta_B \cdot \mu_B \cdot \gamma_B \cdot C_B \tag{22}$$

If the demanded brake force is less than the motor is maximum force, only regenerative brake will be applied to stop the vehicle. Due to the feature that the maximum torque of the traction motor varies under different rpm, the braking torque map has been used to adjust its value. If the demanded brake force is greater than the motor's maximum regenerative braking force, the mechanical brake will supply additional torque to meet the demand. This means that when the braking ratio reaches a certain level, the mechanical brake will be applied to assist regenerative braking to stop the vehicle. However, when the system detects the SOC of the battery pack greater than 90% and SOC of the supercapacitor greater than 80%, only mechanical bakes are applied to

stop the vehicle following the braking strategy curve; this will help to protect the battery and supercapacitor from being damaged by over discharge since the energy store system don't have extra space for absorbing braking energy.

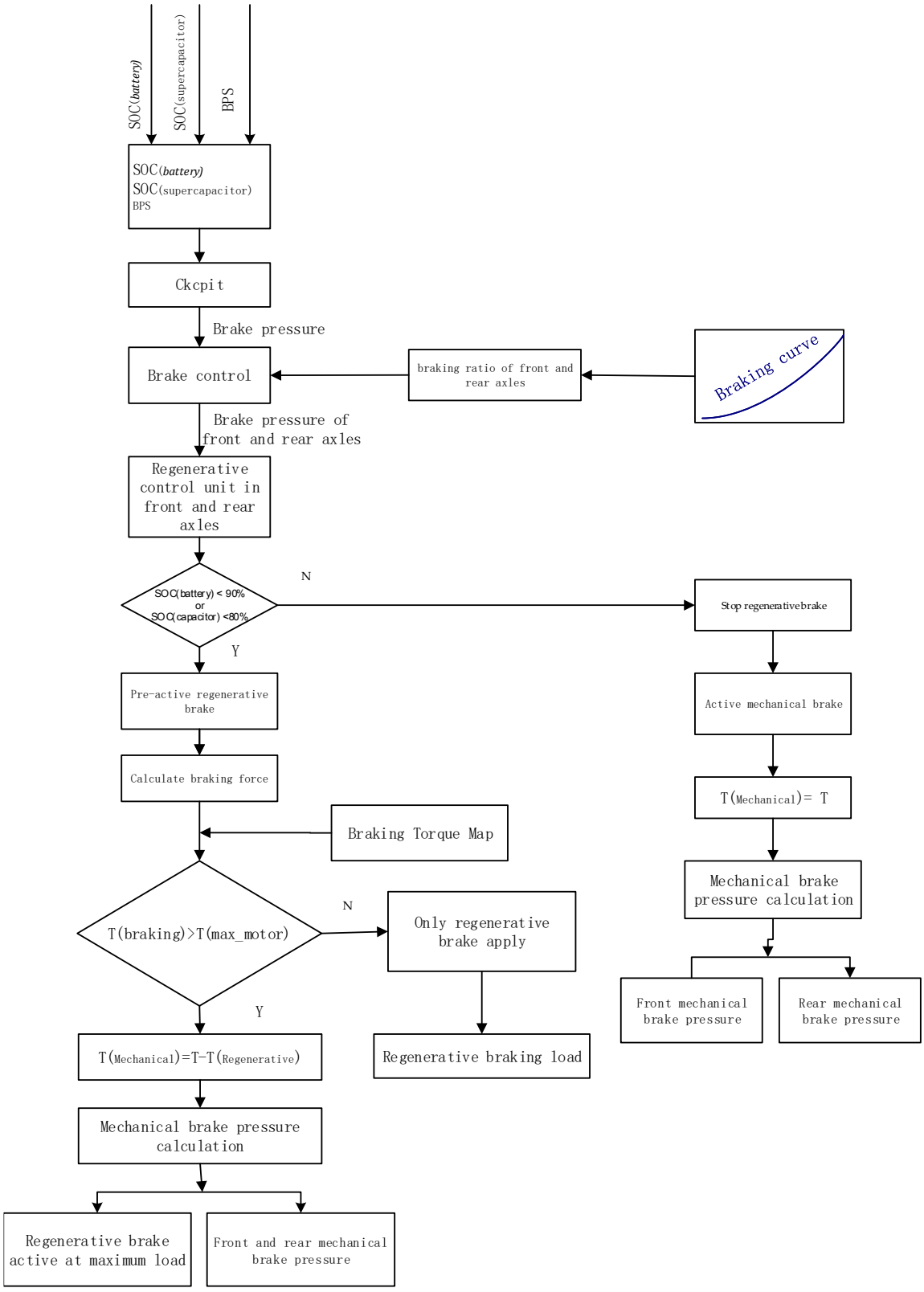

Figure 5.5 Series braking strategy logic -optimal feel

A well design braking system can really make a different to prevent vehicles from collision. This braking control strategy strictly enforces the vehicle braking safety state. Generally, conventional braking system have the same brake pressure output in front and rear axles. That is saying, the front and rear brakes have to use different parameter's disc or drum brake in order to adjust the front and rear braking ratio. The application of this braking strategy provides the flexibility of the brakes size selection since two independent braking control units are used to control the combined braking force of regenerative braking and mechanical braking. Two combined braking forces have been adjusted by a higher-level brakes control unit to match the ideal braking forces distribution. Moreover, the active frequency and loading condition of mechanical have been significantly reduced by only using regenerative braking under low braking load condition. This has certain benefit for preventing the mechanical brakes' wear and extending its durability. All in all, RBS not only offer benefits mechanical braking but also allows the vehicle to have a better fuel efficiency without sacrificing braking safety condition.

CHAPTER 6

VEHICLE ELECTRONIC STSTEM

Hybrid Power Systems

Hybrid power systems basically can be divided into three units: dynamic battery, supercapacitor and DC/DC. The application of the hybrid power system can absorb instantaneous heavy load energy from the regenerative braking system within a short time and increase the energy recuperation rate. The dynamic battery is the main energy store component of the powertrain. It has either a cylindrical shape or a prismatic shape [17]. With respect to hybrid vehicle, the dynamic battery can supply energy to drive the vehicle for around 1-1.5 hours since it has a high specific energy density. However, the dynamic battery has a difficulty in independently satisfying the demanded power of the traction motor since it has a low specific power. When the battery discharge is over the 5C rate, the large discharge currents will damage the battery and affect its SOH. 5C rate means the battery cell discharged with 20 minutes. Moreover, the charge and discharge life cycle of battery is limited. Therefore, with an increase in the number of charges and discharges, the battery SOH will significantly decrease. The ultracapacitor can overcome these issues. It can function as the high specific power supplier and tolerate a high C rate discharge with 98% efficiency. The charge and discharge cycles are almost infinite.

The combination of a dynamic battery and a super capacitor certainly is a better choice to supply more reliable power and energy to drive the vehicle. Topological structure of hybrid power systems generally can be classified into three categories: passive, semi-active and active topology. The designing of hybrid power system should base on the analysis of the calculation, the statistics and the simulation as well as be based on the vehicle dynamic performance and the demanded vehicle driving range [17].

The semi-active topology has been adopted in our all-wheel drive application. The battery and ultracapacitor are series connected and a bio-direction DC/DC equipped between these two power sources, as shown in Figure 6.1. The voltage will be boosted during the current flow from the ultracapacitor to battery to increase the battery charging speed and to reduce the energy lose during charging of the battery. The bio-direction inverter functions as a converter for electricity between 2 phase DC and 3 phase AC [17]. A well-designed hybrid power system should not only have enough energy to drive the vehicle but also can supply high demanded power. As it suggested by Dr. Oriet, the battery pack should store sufficient energy to drive the vehicle 1-1.5 hours and the ultracapacitor size should allow it to supply high instantaneous power within 10-15 seconds.

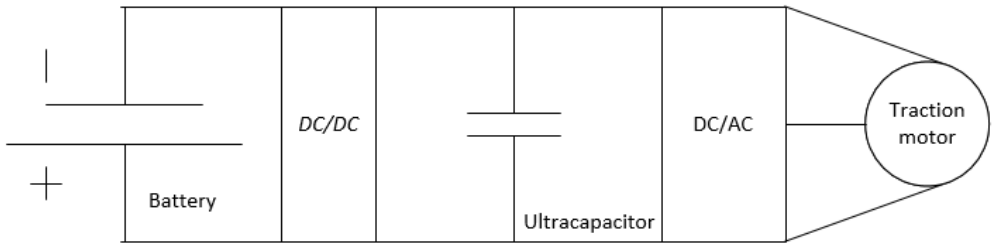

Figure 6.1 Semi-active hybrid power source topology

The DC/DC module is one of the key component of hybrid power system. It functions as an energy manager to supervising the energy flow between the dynamic battery and the ultracapacitor. A well-designed control strategy, the brain of the DC/DC, certainly can improve the whole powertrain efficiency, for the purpose of increasing braking energy recovery rate and extending dynamic battery durability. The bio-DC/DC has been adopted in this hybrid application. The configuration and control logic of DC/DC have been indicated in figure 6.2 and 6.3 respectively. There are three signals that are related to bio-direction DC/DC: drive mode, battery SOC, and ultracapacitor SOC. If the drive mode is on regenerative braking mode, the buck switch will be off

and the boost switch on. Both battery and ultracapacitor function as power source to absorb regenerative braking energy. If the signal is on during the other drive modes, two independent thermostat control strategies will be applied to control the boost, and the buck switch on/off will switch respectively depending on their SOC upper bound and lower bound. This power system design has a significant improvement on battery SOH since the high load current is deal with the ultracapacitor instead of flowing to the battery directly. Based on our DC/DC control strategy, the frequent charge and discharge current can be smoothed in the ultracapacitor to reduce the number of charging and discharging cycles of the battery. This allows the battery longevity to be extended.

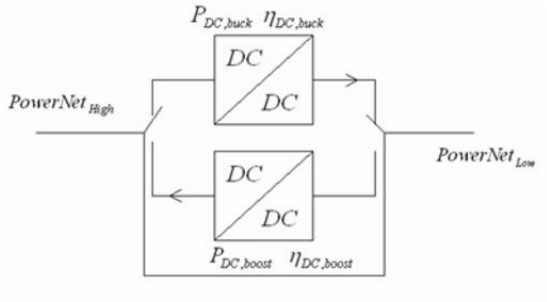

Figure 6.2 Bio-DC/DC configuration [15]

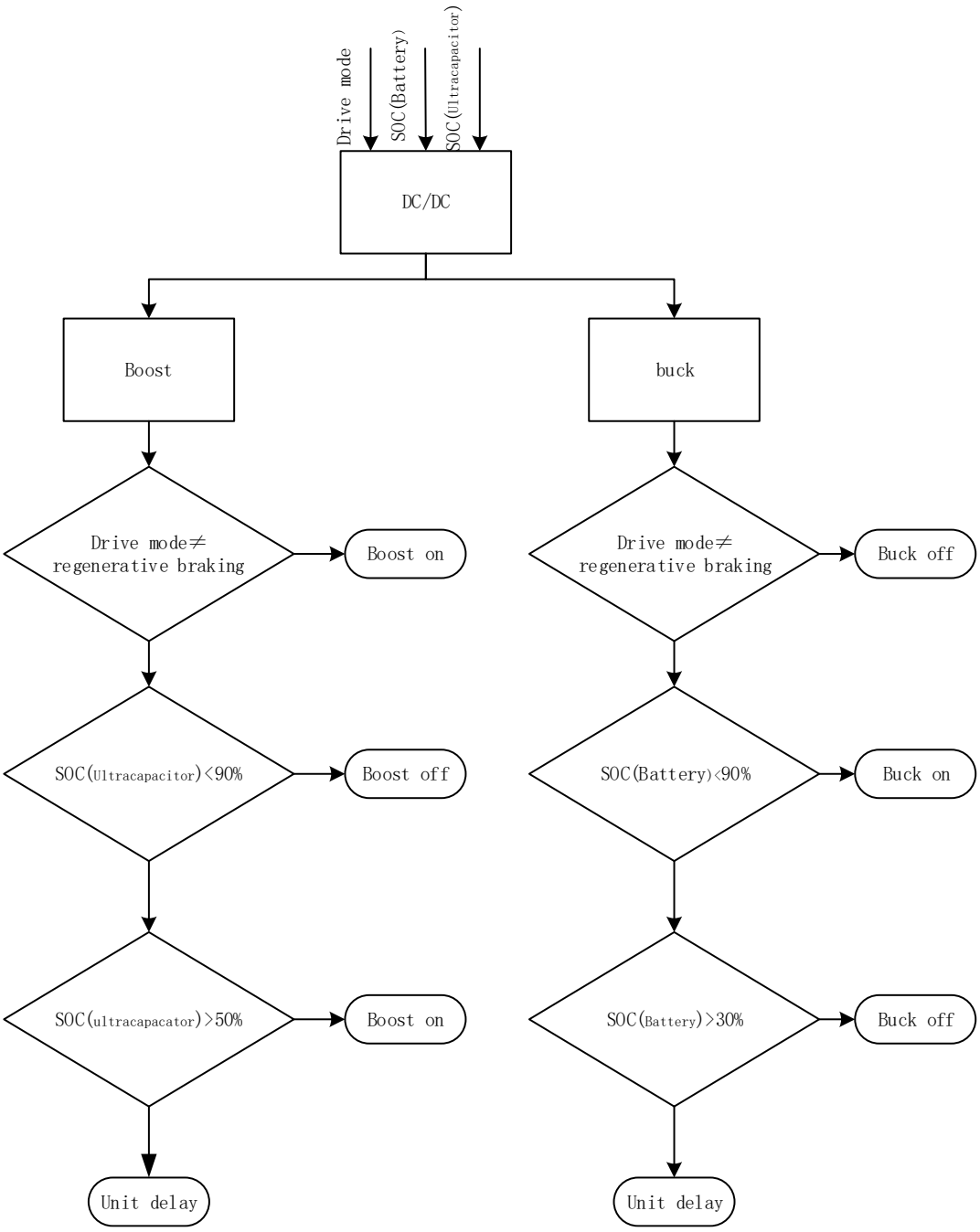

Figure 6.3 Bio-direction DC/DC control logic

Safety Diagnosis

All-wheel drive powertrain has the tremendous advantage of improving the braking energy recovery rate. However, it also has its disadvantages. The more the traction motor drives the

powertrain, the more defective rate of the motor may be exposed. If even one of the motors from the powertrain goes wrong, the vehicle will deviate from original driving direction and cause safety issues. Therefore, safety diagnosis is necessary for the all-wheel drive vehicle to prevent potential hazards in case some components go out of control. The safety diagnosis logic flow is detailed in figure 6.4. The powertrain components which have been monitored will first go through multiple level of the error cognition process in the detect model to judge whether the component is operating under normal conditions [11]. Once the error has been detected, the signal will be sent to the actuator module to shut down related components to prevent safety issues. The primary part of this safety diagnosis design is to prevent the traction going out of control [12]. If one of the motors located in the front axle is out of control, the other motor located in front axle will be shut down. So, the powertrain will be adjusted and be converted to rear drive instead of all-wheel drive. Similarly, if one of the rear traction motor is faulty, the neighbor rear traction motor will shut down resulting in the powertrain changing to front drive. The secondary part of this safety diagnosis design is to prevent the energy loss of the dynamic battery and fuel tank if the ISA or the diesel engine goes wrong. This is means that if either the ISA or the diesel engine goes wrong, both will be shut down and the vehicle will be operating under pure electric vehicle mode to prevent unnecessary energy loss from battery or fuel tank. The logic flow is elaborated in figure 6.4.

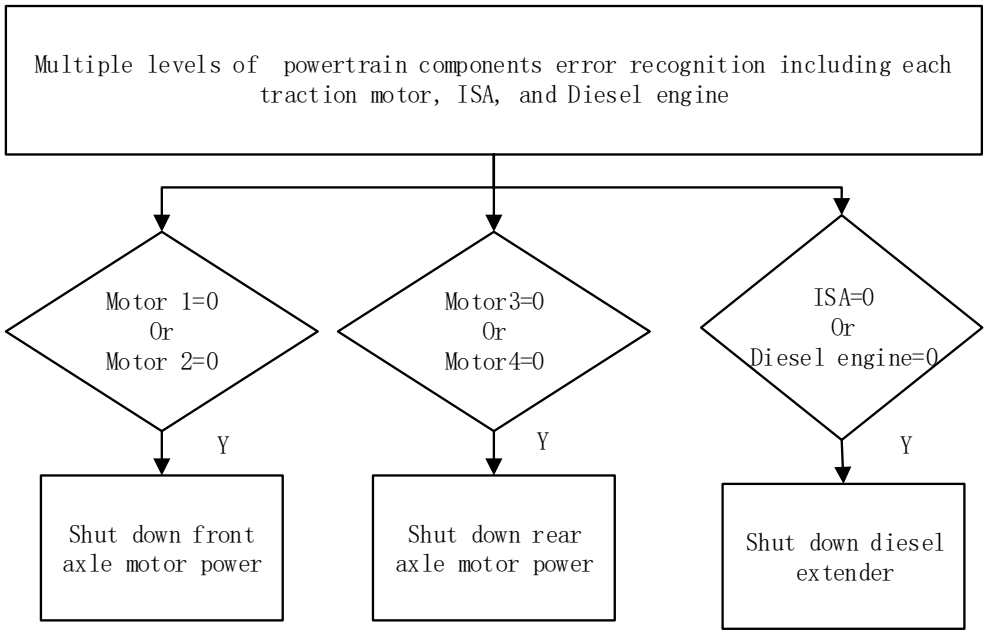

Figure 6.4 Safety diagnosis control logic

CHAPTER 7

RANGE EXTENDER

Engine Efficiency Area Study

In order to convert chemical energy into a usable mechanical energy, the IC engine has to go through a complex combustion process in diesel engines. When the engine operates at each different crankshaft angle degree, adiabatic flame temperature and fuel mass flow rate can vary greatly [7]. Therefore, it is difficult to describe engine operation properly by using mathematical equations. The engine map is the most common and correct method to indicate vehicle fuel consumption since the data of the engine map are obtained from fuel flow rate maps derived from real engine test results [7], as shown in Figures 7.1 and 7.2. The oval-shaped contours from the engine map indicate levels of fuel efficiency [7]. The greatest fuel economy area is located within the center area of the oval-shaped contours [7]. The research of engine efficiency is based on the engine characteristic map study and proposes an appropriate operating condition for the ISA Extender to produce engine work at the engine map high efficiency area.

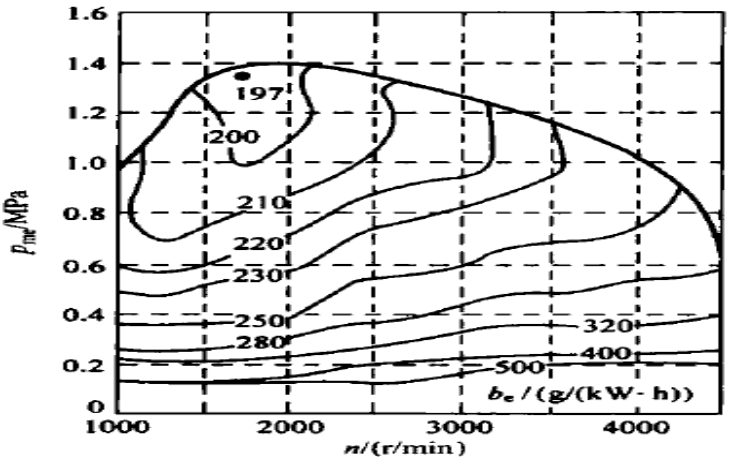

Figure 7.1 Diesel engine map [14]

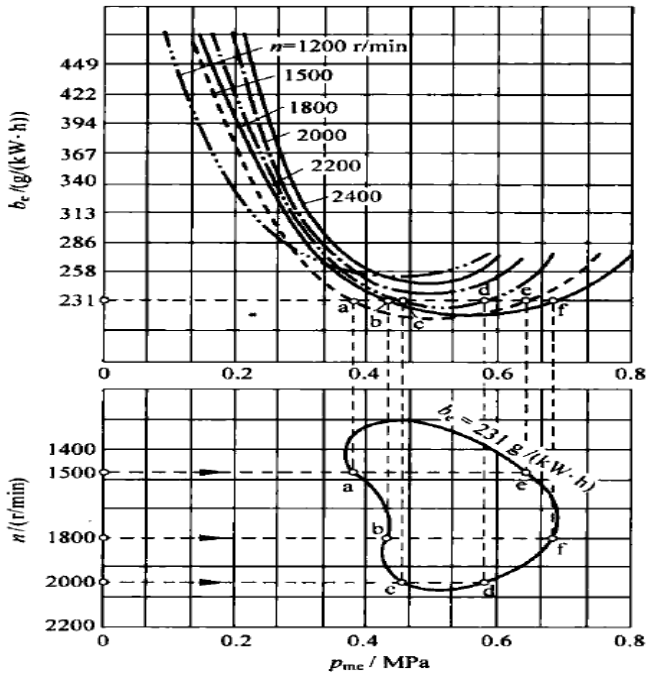

Figure 7.2 Fuel flow rate map [14]

The Control Strategy of Range Extender

Instead of using EGR low temperature combustion technology to reduce the vehicle emission, the hybrid driveline applications generally use a downsized engine to reduce displacement [5]. That is saying the less fuel burnt to produce the same amount of energy, the less GHG emission can be achieved. The objective of our application is to maximum the efficiency of electricity generation and to operate engine under high efficiency conditions. The engine has been controlled to operating under fixed rpm, and the load control of the ISA unit allows the engine to operate under fixed torque [5]. This provides possibility for the engine to operate under the high efficiency area of the engine map [5]. The control logic is elaborated in figure 7.3. When the range extender turn on signal has been sent, the ISA will function as the starter to start rotating the engine crankshaft. After it reach a fixed speed, the engine will start operating the ISA unit switch to the generator mode to control the engine operation in the appropriate load and supply 3 phase for the 3 phase

AC current. The application of the ISA unit also allows the vehicle to start and shut down within a short time as well as eliminate the pollution resulting from engine idling [5].

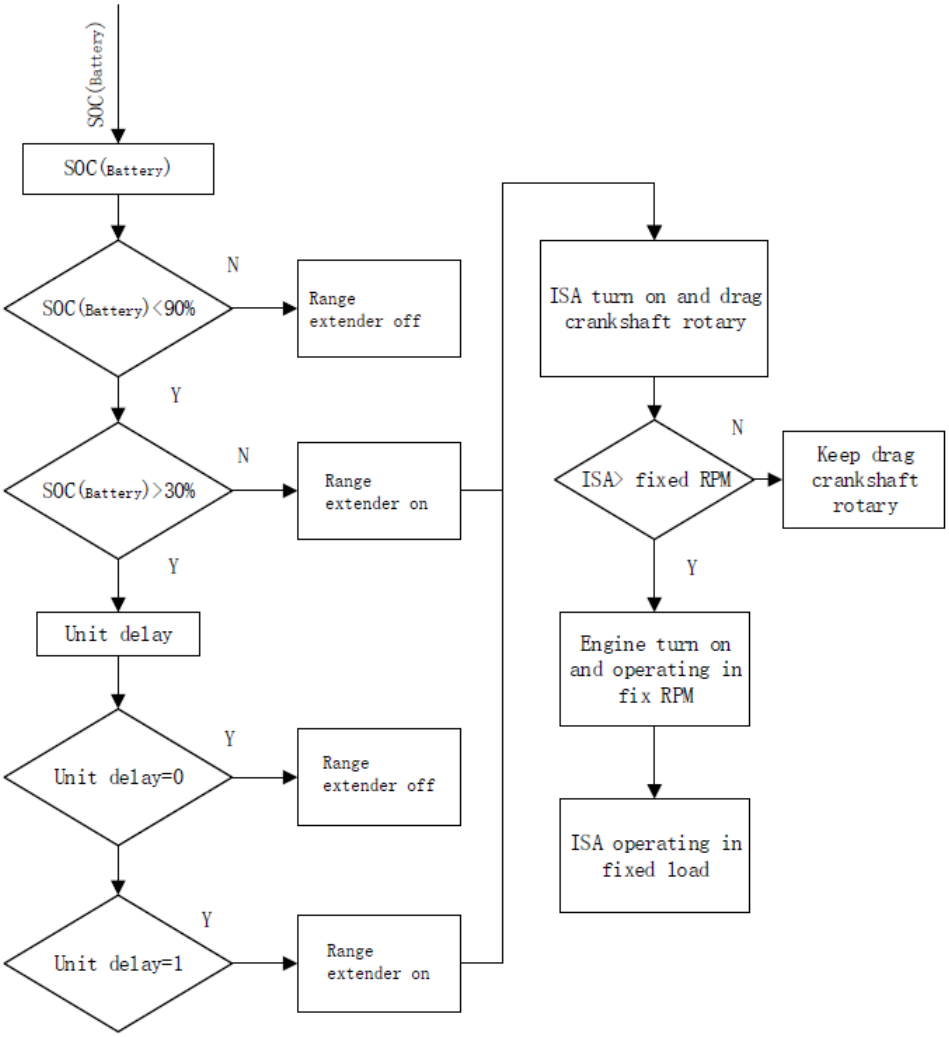

Figure 7.3 ISA range extender control logic

CHAPTER 8

MODELING AND SIMULATION

Modeling of Hybrid Powertrain

The application of this all-wheel drive commercial vehicle was modeled in AVL CRUISE, as it shown in figure 8.1. The specific developed dynamic properties have been update in each hybrid powertrain component modules. The modules are connected by blue or red lines, which represent mechanical and electrical paths respectively [15]. The powertrain control signal path can be construct under the powertrain architecture window. Based on the demanded input and output of control system, the data bus can be set up from here, as it shown in figure 8.2. The on-board control unit has been program in function modules by C style code. The control modules mainly consist of regenerative braking system, anti-lock brakes system control, DC/DC control unit as well as range extender control unit.

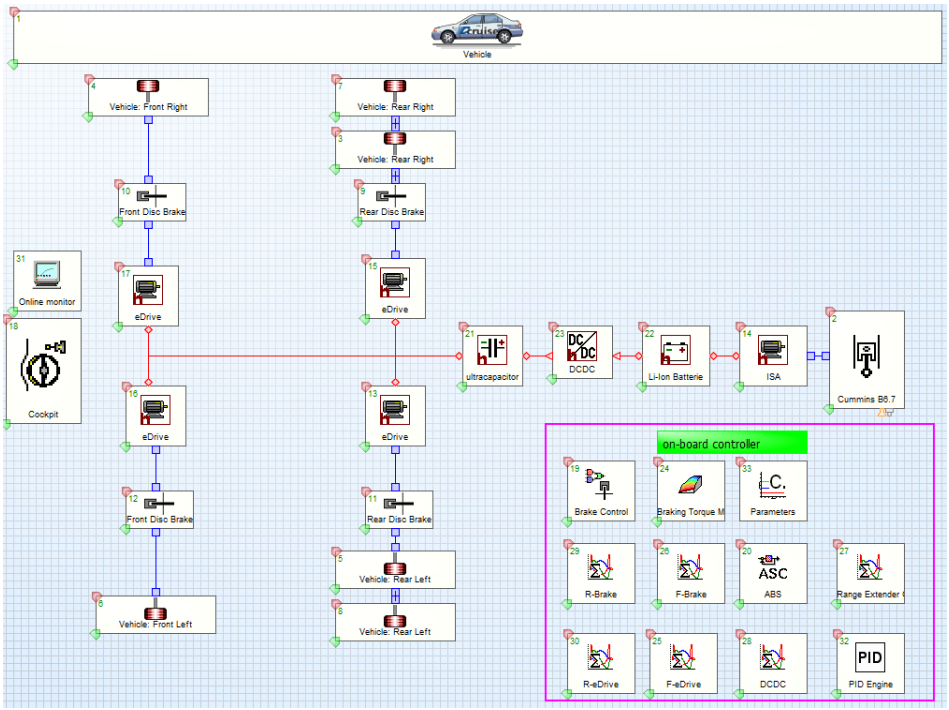

Figure 8.1 All-wheel drive hybrid application configuration

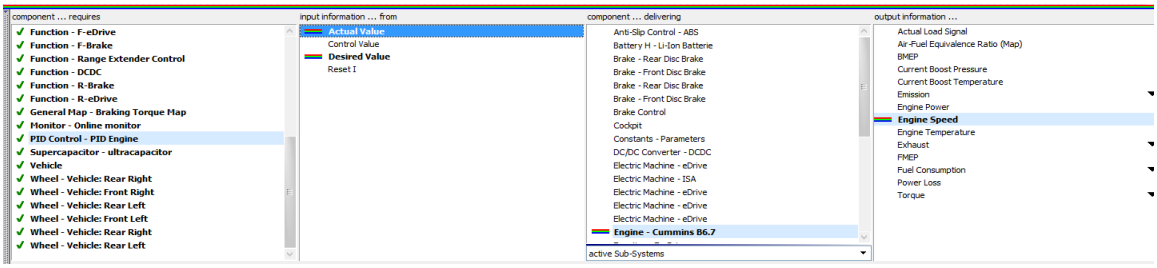

Figure 8.2 Data bus connection window

Simulation Result Analysis

For demonstrating this application, the simulation of all-wheel drive commercial vehicle was made in AVL CRUISE. The model was simulated under the NEDC cycle with a PI controlled driver. As the result indicates this powertrain can either operating under pure electric mode or hybrid mode depending on the SOC level of its dynamic battery as shown in figure 8.3 and 8.4.

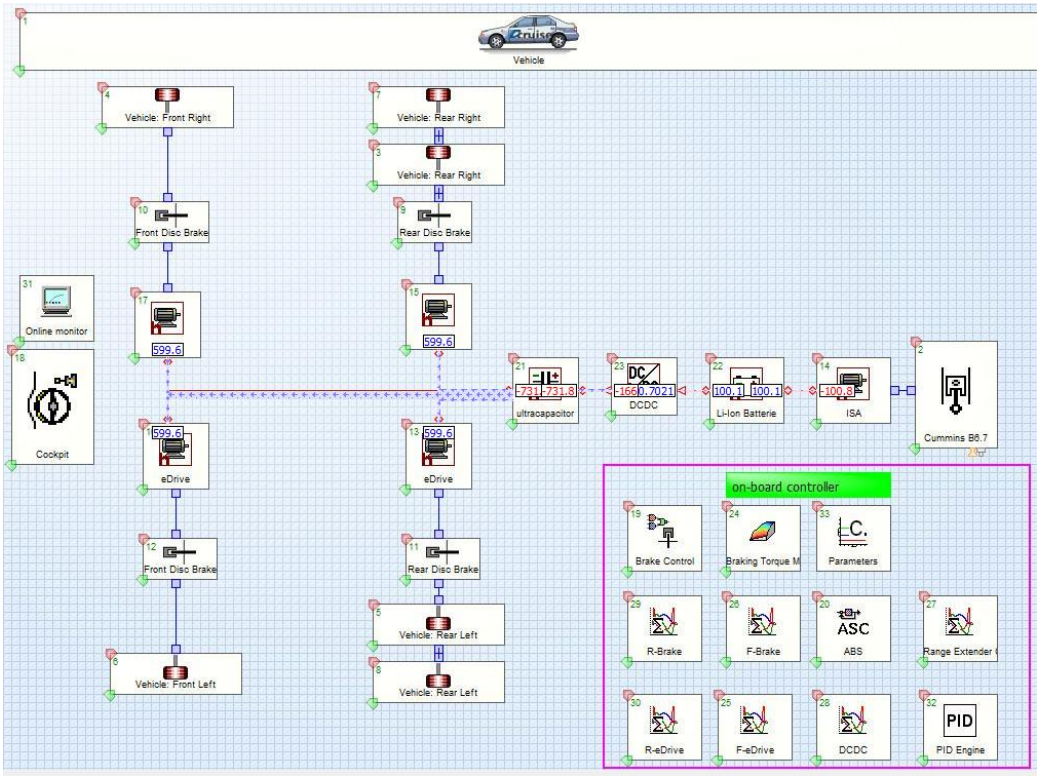

Figure 8.3 Hybrid vehicle mode

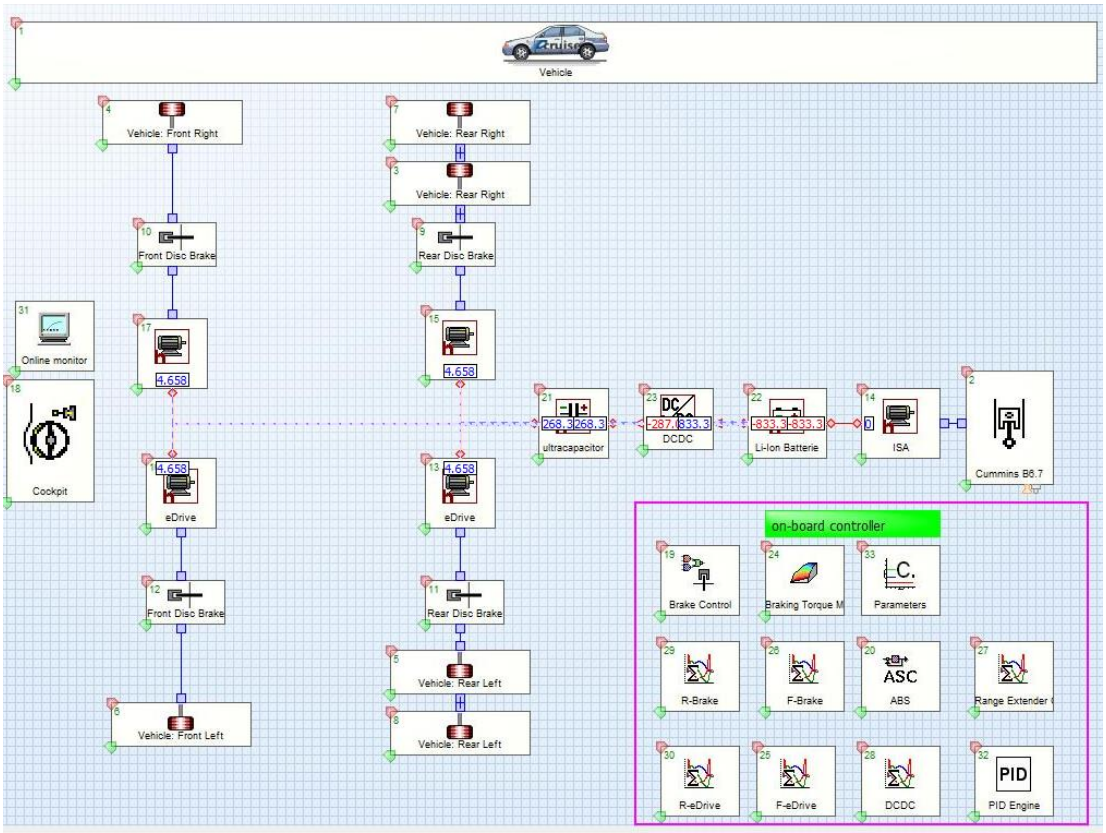

Figure 8.4 Pure electric vehicle mode

With respect to hybrid power source, the ultracapacitor has been used to deal with high load currents and to prevent frequent charge and discharge of the battery. According to figure 8.5 and 8.6, the simulation results indicates that at least 50% of charge cycles has been reduced in the battery charge and discharge operation, compared to the operation condition of ultracapacitor. Moreover, the high load charge current has been smoothed before being sent to charge the battery. This has a significant effect on protecting battery SOH and extending its durability.

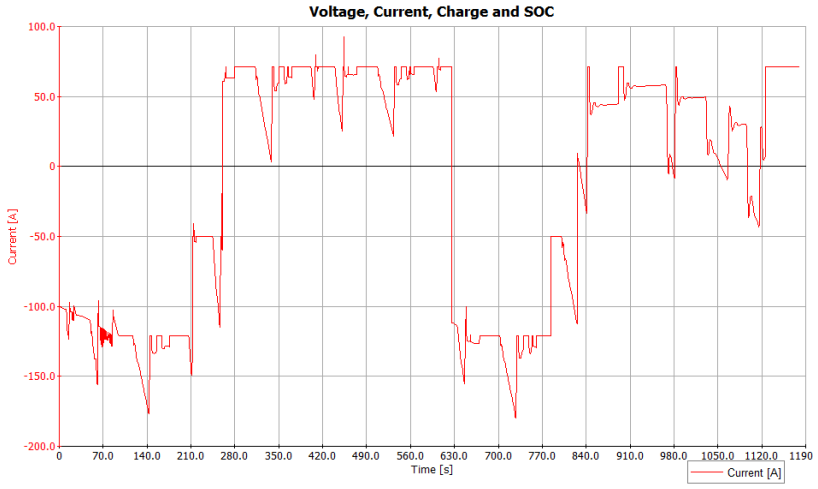

Figure 8.5 Ultracapacitor charge and discharge

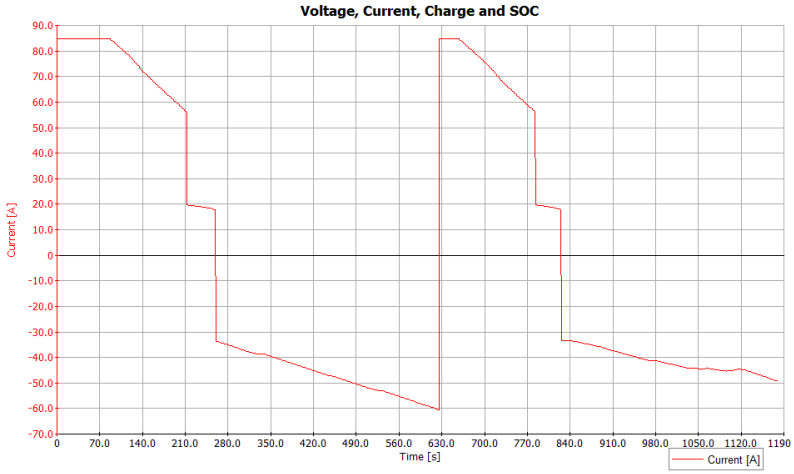

Figure 8.6 Dynamic battery charge and discharge

The engine has been controlled operating under fixed rpm and the load control of the ISA unit allows the engine to operate under fixed torque. In term of engine operating conditions shown in the figure8.7, indicates that the diesel engine controlled to operate under fixed rpm and the load control of the ISA unit allows the engine to operate under fixed torque. Such a control strategy allows the downsized engine to operate with high efficiency. A conventional truck and a rear drive hybrid truck with the same load state were simulated in a steady test drive cycle (NEDC) and a

transient drive cycle (FTP75). these two drive cycles have been define in Tables 2.2 and 2.3. As figures from 8.8 to 8.11 indicate, the cumulated fuel consumption of the conventional truck for NEDC and FTP75 drive cycles are 2.8 liters and 3.5 liters respectively. As a result of regenerative braking technology, the cumulated fuel consumption of the rear drive hybrid truck reduced to 1.75 liters and 2.8 liters. Moreover, the all-wheel drive hybrid application achieved a further progress of fuel efficiency among three type of powertrains. As shown in figures 8.12 and 8.13, 1.2 liters and 1.9 liters of fuel was consumed in NEDC and FTP75. Since the detailed data of the engine could not be obtained from supplier, the fuel consumption results may have a certain discrepancy to the real-world testing. The update data will be loaded into the application model to estimate fuel economy in future development.

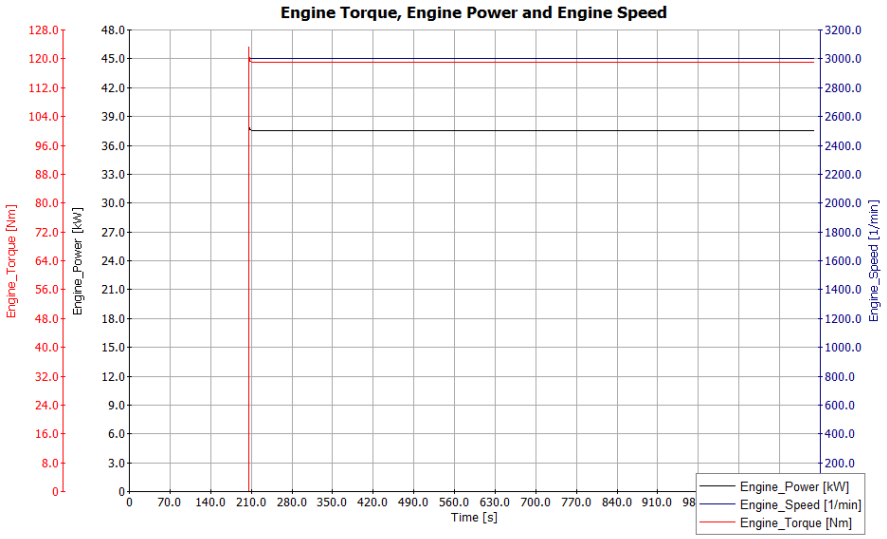

Figure 8.7 Diesel engine operation

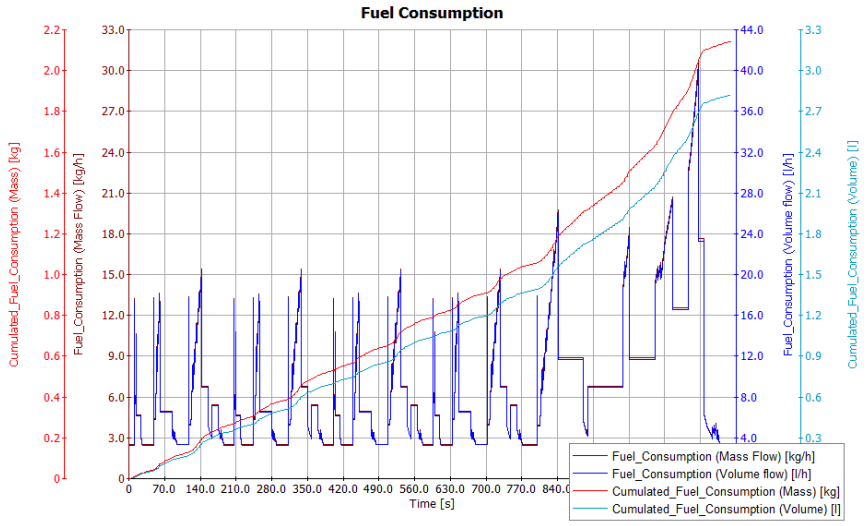

Figure 8.8 The fuel consumption of conventional truck for NEDC drive cycle.

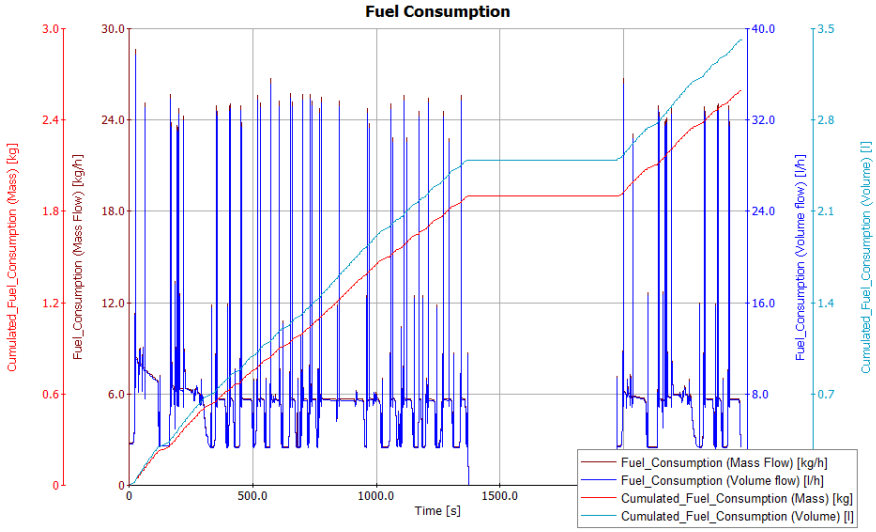

Figure 8.9 The fuel consumption of conventional truck for FTP75 drive cycle.

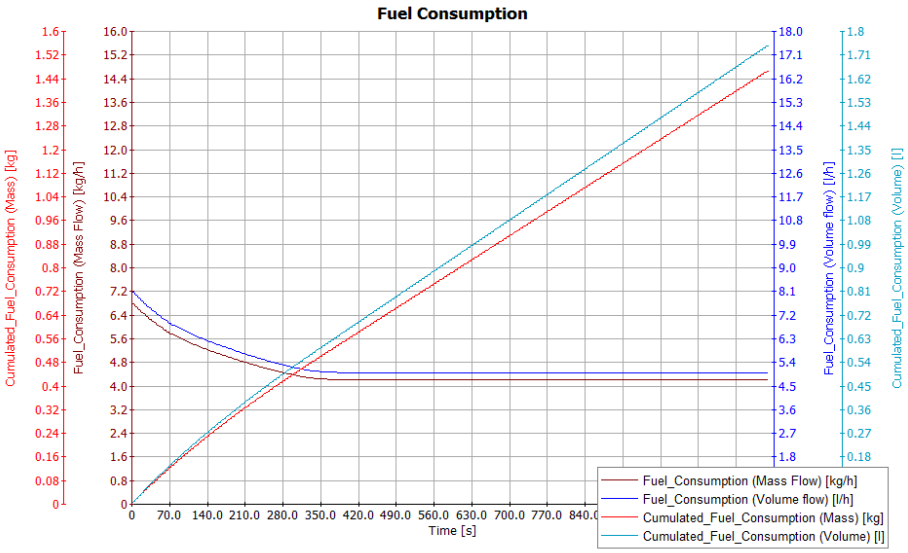

Figure 8.10 The fuel consumption of rear drive hybrid truck for NEDC drive cycle.

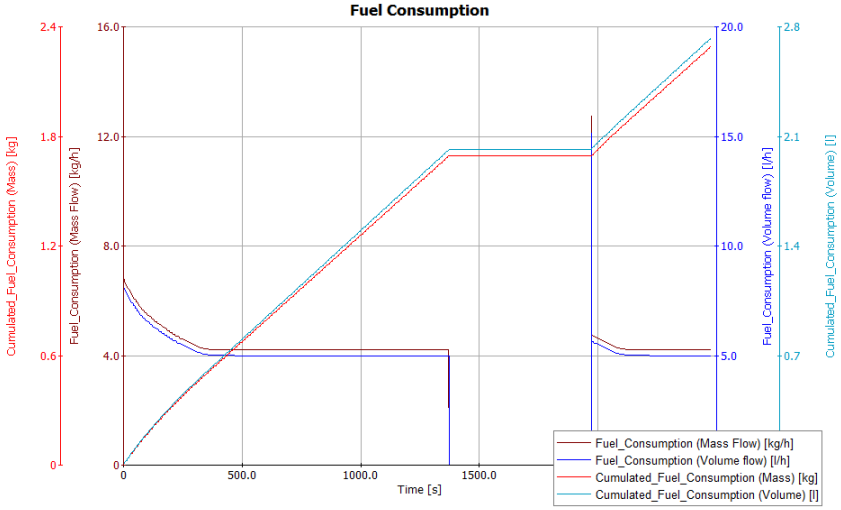

Figure 8.11 The fuel consumption of rear drive hybrid truck for FTP75 drive cycle.

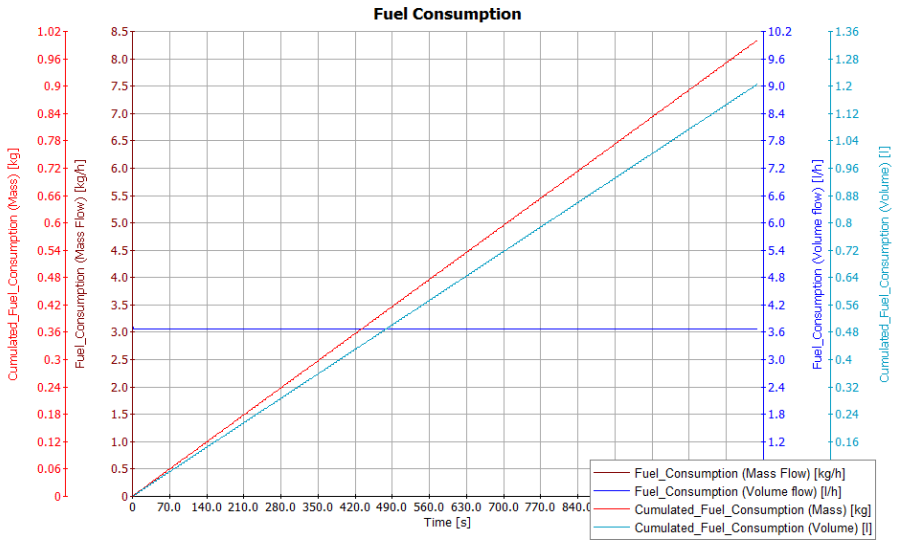

Figure 8.12 The fuel consumption of all-wheel drive application for NEDC drive cycle.

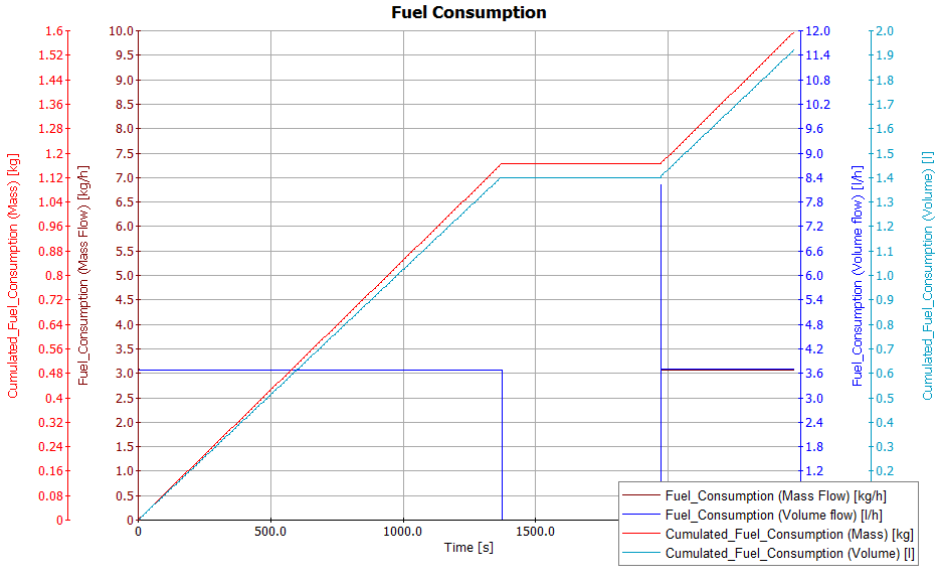

Figure 8.13 The fuel consumption of all-wheel drive application for FTP75 drive cycle.

Last but not the least, the simulation result shows that the traction motor has functioned as the primary vehicle brake and absorbed the kinetic energy loss. The regenerative braking at both front and rear axles had a maximum energy recovery performance during vehicle braking. This

illustrates that the demanded braking force are greater than maximum motor torque under the majority of time of the city driving cycle. The mechanical braking forces at front and rear axles had a huge difference, this indicates the braking forces distribution follows the ideal braking curve to prevent the rear axles lock before the front axle locked. Therefore, this regenerative braking system showed that 61.5% and 95.2% of braking energy lost was recuperated at front and rear axles respectively during vehicle braking, as shown in Figures from 8.14 to 8.17. That is saying, this application has achieved 75% of braking energy recovery rate under the whole powertrain. Compare with up to 40% of energy recovery rate in current commercial vehicles with only rear regenerative braking, it has a dramatic performance in reducing fuel consumption and GHG emission for commercial vehicle.

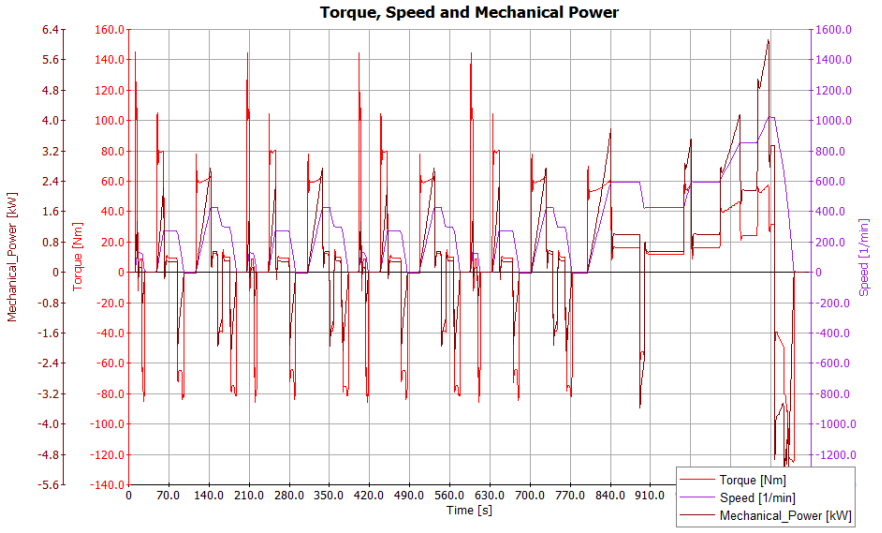

Figure 8.14 Regenerative braking at front axle

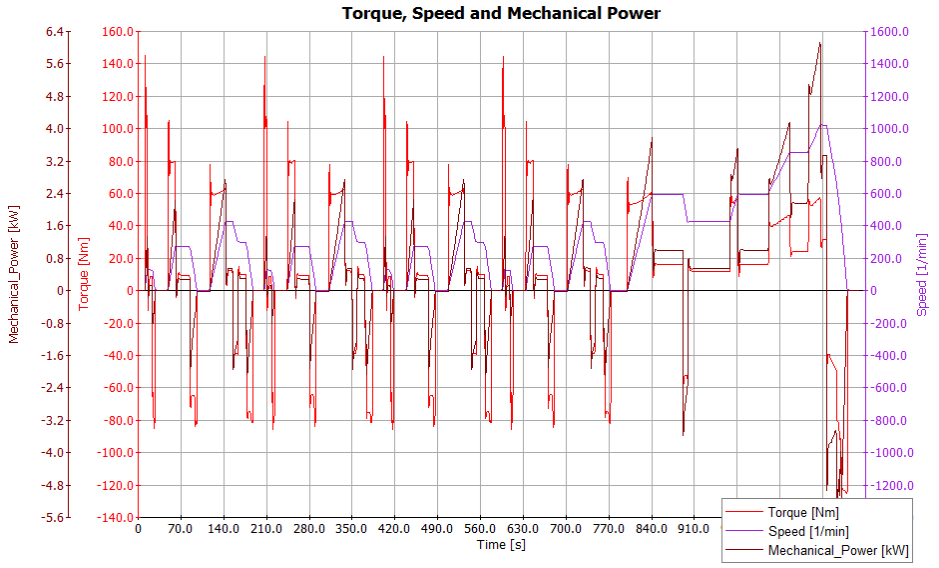

Figure 8.15 Regenerative braking at rear axle

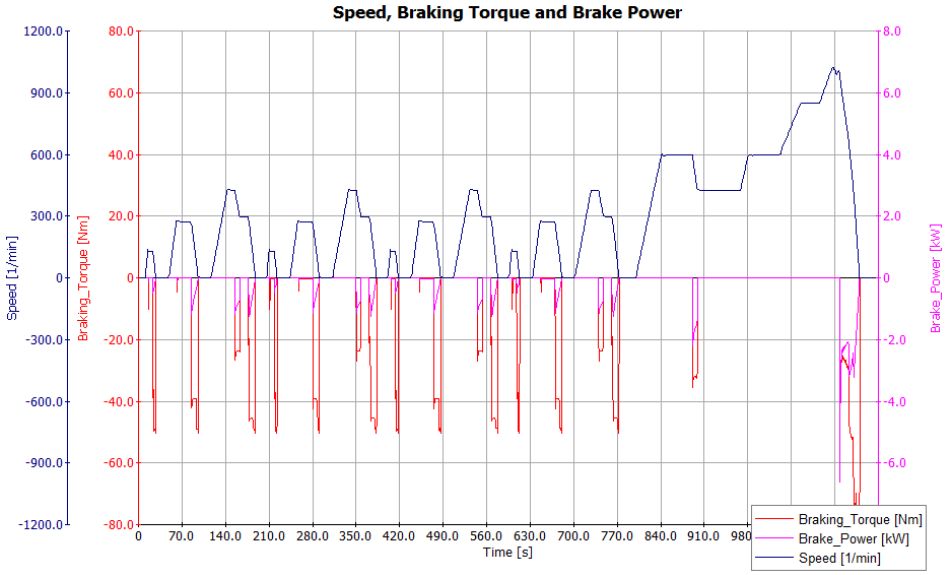

Figure 8.16 Mechanical braking at front axle

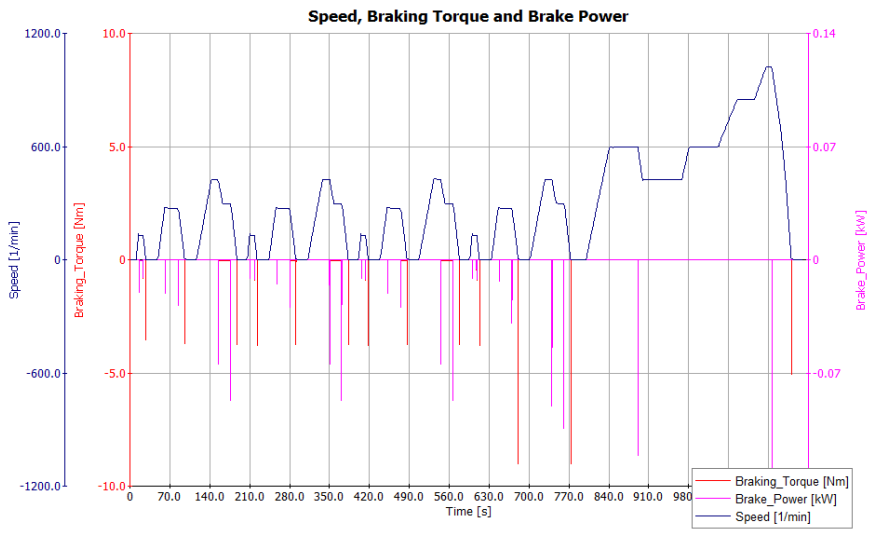

Figure 8.17 Mechanical braking at rear axle

Design of Experiment(DoE)

In order to achieve a desired objective of fuel consumption and emission, design of experiment is irreplaceable in powertrain calibration. Three scales of treatments of DoE plan is available in AVL CRUISE: Single variable level; component variable level; system variable level. Single variable is use for testing component parameter. Component variable is use to test for component products; system variable is use to the vehicle configurations. The DoE plans has been establish as shown below.

DoE plan 1 is to test the electricity generation efficiency. As an internal changer of the battery, ISA and IC engine matching is meaningful for reducing GHG emission since twice the energy conversion occurs during charging the battery. It is necessary to optimize the efficiency of the electricity generation. Consequently, three type generators and five types of diesel engine were selected and established 15 DoE cases. Component variable has been used in this DoE plan. Engine and generator models are adjusted to the same initial state and fuel property in order to generate a precise simulation result. Moreover, the generator output state of current and speed

should be under unlimited condition, in case of maximize the energy yield. According to the DOE cubes (Figure8.18), the engine selection has a more interaction effect on emission reduction, compared to the generator selection. As shown in Figure 8.19, though the NOX, CO, and HC emissions of the match between IC6C6.8L and M288V55T is slightly higher than the match between IC6C6L and M288V55T, it is the best choice in terms of fuel efficiency and GHG reduction.

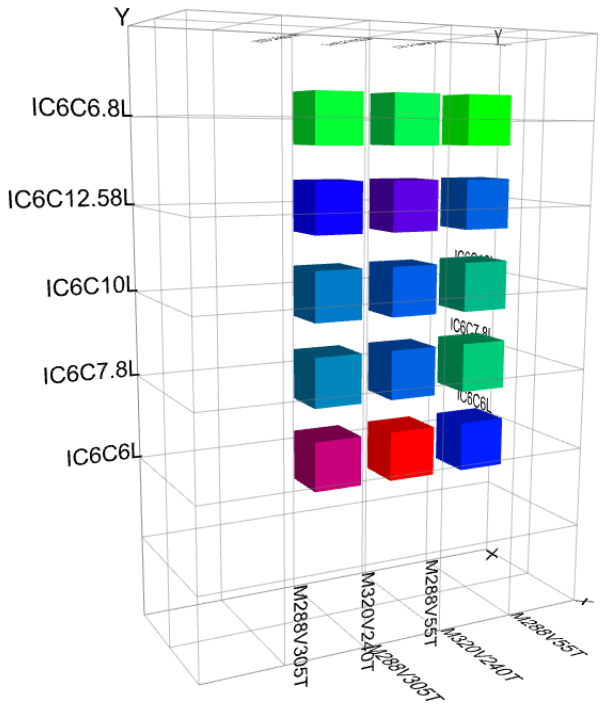

Figure 8.18 The comparison cubes of DoE plan 1.

Variation of Engine	Variation of Electric Machine	NEDC (2/1) Consumption <l/100km>	NEDC (2/1) Way-dependent Emissions CO2 <g/km>	NEDC (2/1) Way-dependent Emissions NOx <g/km>	NEDC (2/1) Way-dependent Emissions CO <g/km>	NEDC (2/1) Way-dependent Emissions HC <g/km>
IC6C6L	M288V55T	22.94	600.37	0.28	2.88	0.53
IC6C6L	M320V240T	38.77	1014.66	1.82	5.21	1.01
IC6C6L	M288V305T	33.35	872.77	1.19	4.37	0.83
IC6C6.8L	M288V55T	9.91	259.36	1.17	6.46	0.75
IC6C6.8L	M320V240T	13.38	350.21	3.08	9.01	1.29
IC6C6.8L	M288V305T	12.2	319.43	2.35	8.04	1.07
IC6C7.8L	M320V240T	19.97	522.59	4.2	13.35	1.84
IC6C7.8L	M288V305T	18.36	480.59	3.28	11.94	1.55
IC6C7.8L	M288V55T	15.24	398.97	1.72	9.95	1.16
IC6C10L	M288V55T	16.11	421.57	1.69	10.62	1.23
IC6C10L	M320V240T	20.21	528.88	3.71	13.21	1.73
IC6C10L	M288V305T	18.83	492.91	2.94	12.02	1.49
IC6C12.58L	M320V240T	28.49	745.75	36.8	0	0
IC6C12.58L	M288V305T	24.86	650.66	36.8	0	0
IC6C12.58L	M288V55T	19.85	519.45	36.79	0	0

Figure 8.19 The result of DoE plan 1for NEDC drive cycle

Variation of Engine	Variation of Electric Machine	FTP75 (2/2) Consumption <l/100km>	FTP75 (2/2) Way-dependent Emissions CO2 <g/km>	FTP75 (2/2) Way-dependent Emissions NOx <g/km>	FTP75 (2/2) Way-dependent Emissions CO <g/km>	FTP75 (2/2) Way-dependent Emissions HC <g/km>
IC6C6L	M288V55T	22.51	589.18	0.28	2.83	0.52
IC6C6L	M320V240T	37.99	994.25	1.79	5.11	0.99
IC6C6L	M288V305T	32.66	854.81	1.17	4.27	0.81
IC6C6.8L	M288V55T	9.7	253.93	1.15	6.33	0.74
IC6C6.8L	M320V240T	13.1	342.77	3.01	8.84	1.26
IC6C6.8L	M288V305T	11.94	312.52	2.3	7.88	1.05
IC6C7.8L	M320V240T	19.54	511.49	4.11	13.1	1.8
IC6C7.8L	M288V305T	17.97	470.23	3.21	11.71	1.51
IC6C7.8L	M288V55T	14.93	390.65	1.68	9.75	1.13
IC6C10L	M288V55T	15.77	412.77	1.65	10.4	1.21
IC6C10L	M320V240T	19.78	517.74	3.63	12.95	1.69
IC6C10L	M288V305T	18.43	482.37	2.87	11.77	1.45
IC6C12.58L	M320V240T	27.99	732.47	35.96	0	0
IC6C12.58L	M288V305T	24.42	639.13	35.96	0	0
IC6C12.58L	M288V55T	19.54	511.39	35.95	0	0

Figure 8.20 The result of DoE plan 1for FTP75 drive cycle

DoE plan 2 tested whether traction motor variation affects vehicle emission. Based on the simulation result (Figure 8.21 and 8.22), the factor of traction motor does affect fuel consumption. DoE of component variable level has been executed in the plan 2. The M320V240T case has a better fuel efficiency than M288V305. This may because a higher voltage of motor helps reduces the energy lose. Due to the lack of adequacy of motor models, further investigation need be carried out to validate more findings.

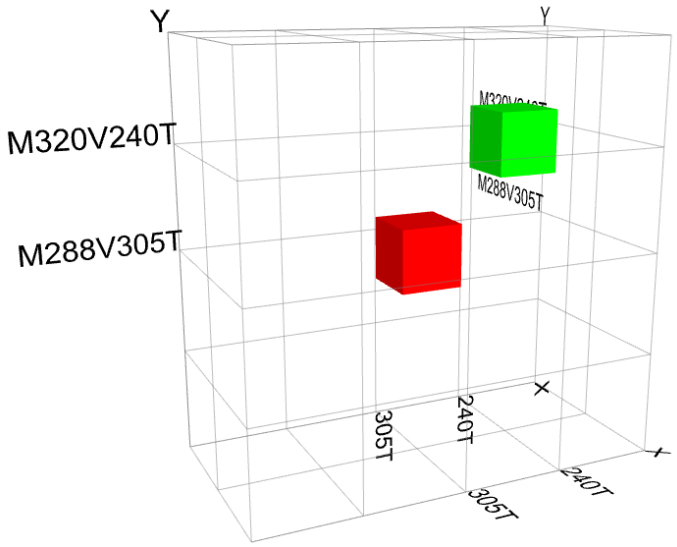

Figure 8.21 The comparison cubes of DoE plan 2

Variation of Electric Machine	NEDC (2/1) Consumption <l/100km>	NEDC (2/1) Emissions CO2 <g>	NEDC (2/1) Way-dependent <g/km>	NEDC (2/1) Way-dependent <g/km>	FTP75 (2/2) Consumption <l/100km>	FTP75 (2/2) Way-dependent <g/km>	FTP75 (2/2) Way-dependent <g/km>	FTP75 (2/2) Way-dependent <g/km>	FTP75 (2/2) Way-dependent <g/km>
M320V240T	9.91	2833.94	259.34	6.46	9.7	253.93	1.15	6.33	0.74
M288V305T	9.92	2833.95	259.65	6.47	9.88	258.66	1.17	6.45	0.75

Figure 8.22 The result of DoE plan 2

With respect to DoE plan 3, it has been assumed that the transmission ratio of the single transmission can affect the powertrain efficiency and single variable level DoE is used by this DoE plan 3. The transmission ratio factors set up from 1 to 10, which can cover the entire range of a single transmission. If a single transmission is needed, the appropriate transmission ratio would be indicated in the DoE cubes. However, as shown in Figure 8.23 and 8.24. the DoE result of the steady driving cycle test shows that direct motor driving would be the best choice, compared to adding the single ratio transmission. Also, the transient test cycle indicates that the variable didn't affect the response of the DoE plan. Therefore, the previous hypothesis was disproved.

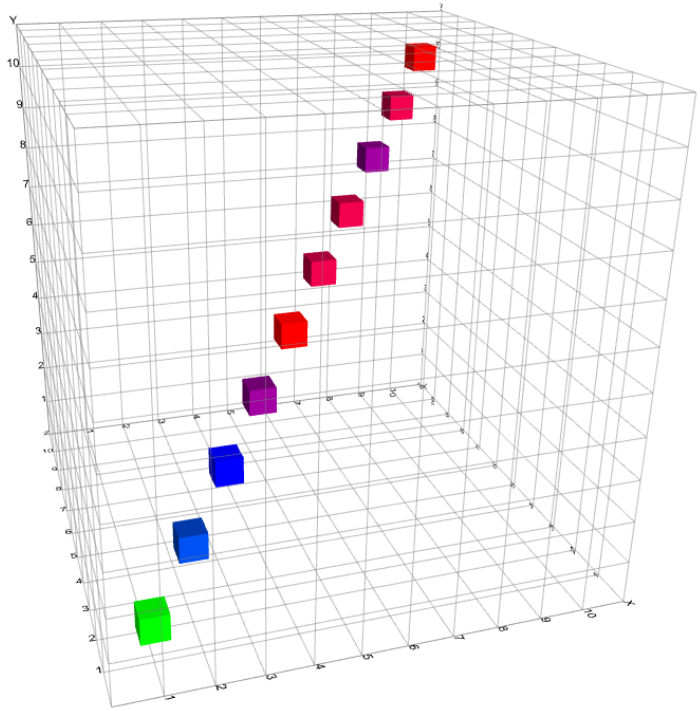

Figure 8.23 The comparison cubes of DoE plan 3

Variation of tr1	Variation of tr2	Variation of tr3	Variation of tr4	Variation of Transmission Ratio of Single Ratio Transmission	NEDC (2/1) Consumption <l/100km>	NEDC (2/1) Way-dependent Emissions CO2 <g/km>	FTP75 (2/2) Consumption <l/100km>	FTP75 (2/2) Way-dependent Emissions CO2 <g/km>
1	1	1	1	1	9.91	259.34	9.7	253.93
2	2	2	2	2	9.91	259.38	9.7	253.96
3	3	3	3	3	9.91	259.4	9.7	253.97
4	4	4	4	4	9.91	259.4	9.7	253.99
5	5	5	5	5	9.91	259.41	9.7	254.01
6	6	6	6	6	9.91	259.41	9.7	254
7	7	7	7	7	9.91	259.41	9.7	254
8	8	8	8	8	9.91	259.42	9.7	253.99
9	9	9	9	9	9.91	259.46	9.7	254
10	10	10	10	10	9.91	259.45	9.7	254.01

Figure 8.24 The result of DoE plan 3

CHAPTER 9

THESIS CONCLUSION

Model based development plays an indispensable role in the powertrain design and calibration for the automotive industry. A good simulation model can not only test whether the control logic is applicable but also experiment to determine whether the overall powertrain components function together efficiently. In order to improve fuel efficiency for hybrid commercial vehicle, it is essential to boost the regenerative energy rate. In order to achieve the objective of improving kinetic energy recovery rate, the powertrain parameters were first calculated to propose its vehicle dynamic performance for all-wheel drive application, then the characteristic of mechanical braking and regenerative braking were analyzed. In case of matching the data with calculation and analysis, the author collected the engine data, motor data, as well as battery data in many ways. On the strength of the collected data, the model of this all-wheel drive hybrid configuration was created. Meanwhile, The hybrid control unit was integrated into function modules. the simulation model was executed in AVL CUISE. to demonstrate its fuel efficiency improvement, two comparison models were simulated including a conventional truck with 16 speeds transmission and a series hybrid vehicle with the rear motor drive system. Furthermore, three DoE plans were executed to further to refine the model and improve its fuel efficiency. This simulation result demonstrates that the majority of braking energy was recuperated; its fuel efficiency has a dramatic improvement; the frequency of mechanical braking usage has been reduce; the battery charging and discharging cycles decreased. The presented model and simulation results have demonstrated the all-wheel drive hybrid application of the regenerative braking system and its braking control logic results in significant improvement in fuel economy and reducing GHG emission.

Due to being unable to obtain the powertrain component data from suppliers, some of the powertrain parameters in this application need to be further adjusted in order to get a more precise simulation and to validate its fuel consumption. Moreover, the author found that the MIL simulation unable to deactivate some modules during computing. Regarding with this case, the diagnostic function module wasn't integrated into the presented simulation model. The current study highly relied in data from MIL simulation, future research need to be carried out under HIL simulation environment in case of investigating more findings.

REFERENCES/BIBLIOGRAPHY

[1] Ehsani,M. Gao,Y. Sebastien,E. Emadi,A. "Modern electric, hybrid electric, and fuel cell vehicles: fundamentals, theory, and design," (CRC Press, 2004), ISBN: 978-1-4200539-8-2.

[2] Liu,W. "Introduction to Hybrid Vehicle System Modeling and Control" Wiley Press,2013, ISBN 978-1-118-30840-0

[3] Reza N. Jazari, "Vehicle Dynamics: Theory and Application," Springer press,2008, ISBN: 978-1-4614-8544-5.

[4] Ciro,A." Electrical Aspects of Hybrid Electric Vehicles," University of Michigan, ECE5462

[5] Leo P. Oriet, "Series Hybrid Generator," U.S. Patent No. 20150008055A1. Jan 8, 2015.

[6] Leo P. Oriet, "Structural electric tandem axle module," U.S. Patent No.0090505. Apr. 2, 2015.

[7] Zhang,Y. Oriet,L. Lang,E. Bhovsar,D. and Tang,Z. "Hybrid Powertrain Parameter Optimization and High Efficient Area Matching of Engines Exclusive to Hybrid Commercial Vehicles,"ACTA MECHANÌCA ET MOBILITATEM, Vol. 2(3), pp. 21—26

[8] Zhang,Y. Oriet,L. Lang,E. and Tang,Z. "The Application of Regenerative Braking System to the Commercial Hybrid Vehicles with All-Wheel Drive System", in Proceedings of the AVL International Simulation Conference 2017, Graz, AT, Jun. 2017.

[9] Bhovsar,D. Tang,Z. Zhang,Y. Oriet,L. And Lang,E. "Methodology and initial analysis to compare hydraulic hybrid and electric hybrid for commercial vehicle," ACTA MECHANÌCA ET MOBILITATEM, Vol. 1(1), pp. 6—10

[10] Ulsoy,G. Peng,H. Çakmakci,M. "Automotive Control Systems," Cambridge University Press,1 edition,ISBN-10: 1107686040

[11] Martin,K." Plug-in Hybrid Electric Vehicle Control Strategies Utilizing Multiple Peaking Power Sources" University of Windsor Thesis.2010.

[12] Chris, M. Masrur, David,A. Gao,W." Hybrid Electric Vehicles: Principles and Applications with Practical Perspectives," Wiley press,2011,ISBN-10: 0470747730

[13] Wang,W. "Optimization Design and Control of Dual-Voltage HEV Compound Power Based on Analysis of Thermal Characteristics," Jilin University Thesis,2015

[14] Yu,Z "Vehicle Dynamics," China: China machine press, 2009, ISBN: 9787111020769

[15] AVL CRUISE Users Guide

[16] Williamson,S."Energy Management Strategies for Electric and Plug-in Hybrid Electric Vehicles".Springer Press.2013.Concordia University.Montreal. QC.ISBN 978-1-4614-7710-5.

[17] Martin,K.” Plug-in Hybrid Electric Vehicle Control Strategies Utilizing Multiple Peaking Power Sources” University of Windsor.2010.

[18] Omara, A. Sleptsov,M."Comparative Study of Different Electric Propulsion System Configurations Based on IPMSM Drive for Battery Electric Vehicles"

[19] Golla,S.Keskar,H.and Kale,M. "Antilock Braking System Modeling and Develoment" Vehicle Dynamics.ME5670.Indian Institute of Technology, Hyderabad.

[20] Hébert,B. Lagos,J. "Power Generation in Canada" published by Canadian Electricity Association.Ottawa, Ontario. 2006

[21] Pundir,BP." Engine Emissions and Air Pollution" Indian Institute of Technology Kanpur. Engine Emission course. August. 2017.

[22] Pundir,BP." Emission Test Procedures" Indian Institute of Technology Kanpur. Engine Emission course. August. 2017.

[23] Pundir,BP." Emission Standards "Indian Institute of Technology Kanpur. Engine Emission course. August. 2017.

[23] ECOpoint Inc" Emission Test Cycles Handbook" DieselNet.April.2017.

[24] AVL List GmbH " AVL Emissions Measurement Solutions Handout" Graz, Austria. November.2016

[25] MERITOR WABCO"Anti-LockBraking System Training Program-Student Manual"ArvinMeritor,Inc.MI.USA.1999

[26] International DuraStar Series-Medium Conventional Body Builder Handbook. October, 2010

[27] AVL List GmbH "AVL CONCERTO™ Road Converter Handout" Graz, Austria. November.2016

[28] AVL List GmbH "AVL Emission Testing Handbook 2016"Graz, Austria. November.2016

[29] Hyderabad"ANTILOCK BRAKING SYSTEM MODELING AND DEVELPOMENT

[30] Rizzoni,G."Driving Cycles" ME7384. The Ohio State University.Autumn.2015.

[31] Shazly,M."Brakes & Braking Behaviour" Faculty of Engineering.The British University in Egypt.2014

[32] Kooijman,D. Ligterink,N "WLTP Random Cycle Generator"Research Gate.October. 2015.DOI: 10.1109

[33] Broustail,G. Ananthan,S."Model Based Development and Calibration" AVL UK Expo. Feb. 2015

APPENDICES

Appendix A

Function-F-eDrive

```
/*

The required channel data are indicated below:

a[0] : Vehicle Velocity

a[2]: Load Signal

a[3]: Brake Pressure

a[6]: Motor Characteristic Map

a[7]: Specific Brake Factor-Front

a[8]: Efficiency-Front

a[9]: Transmission Ratio of Single Ratio Transmission

a[12]: Front Piston Surface

a[13]: Effective Friction Radius

a[14]: Friction Coefficient-Front

a[15]:Battery SOC

a[16]:Supercapacitor SOC

a[17]: constant(-1)

y[0]: Load Signal

*/

if ((a[3] > 0 && a[0] >0.1) && (a[15]<90 || a[16]<80))

{

if(2*a[3]*a[12]*a[7]*a[8]*a[17]a[13]*a[14]/a[9]< a[6])

{

y[0]=-1;

}
```

```
else
{
y[0]=2*a[3]*a[12]*a[7]*a[8] *a[13]*a[14]/a[9]/a[6];
}
}
else
{
    y[0] = a[2];
}
```

Appendix B

Function-F-Brake

```
/*
The required channel data are indicated below:
a[0]: eDrive Torque
a[1]: Transmission Ratio of Single Ratio Transmission
a[5]: brake pressure input
a[6]: Brake Piston Surface-Front
a[7]: Specific Brake Factor-Front
a[8]: Efficiency-Front
a[9]: Effective Friction Radius
a[10]: Friction Coefficiency-Front
a[11]: Battery SOC
a[12]: Supercapacitor SOC
y[0]: brake pressure output
*/
```

```
if (a[0] < 0&&(a[11]<90 || a[12]<80))
{
   eBrake = 2*a[0]*a[1]/(2*a[6]*a[7]*a[8]*a[9]*a[10]);
}
else
{
    eBrake = 0.;
}
if ((eBrake+a[5])>0.0)
{
    y[0]= (eBrake+a[5]);
}
else
{
    y[0]= 0.0;
}
```

Appendix C

Function-R-eDrive

```
/*
The required channel data are indicated below:
a[0] : Vehicle Velocity
a[2]: Load Signal
a[3]: Brake Pressure
a[6]: Motor Characteristic Map
a[9]: Transmission Ratio of Single Ratio Transmission
```

```
a[12]: constant(-1)

a[13]:Battery SOC

a[14]:Supercapacitor SOC

a[15]: Specific Brake Factor-Rear

a[16]: Efficiency-Rear

a[17]: Rear Piston Surface

a[18]: Effective Friction Radius

a[19]: Friction Coefficient-Rear

y[0]: Load Signal

*/

if ((a[3] > 0 && a[0] >0.1) && (a[13]<90 || a[14]<80))

{

if(2*a[3]*a[12]*a[15]*a[16]*a[17]a[18]*a[19]/a[9]< a[6])

{

y[0]=-1;

}

else

{

y[0]=2*a[3]*a[15]*a[16]*a[17]a[18]*a[19]/a[9]/a[6];

}

}

else

{

    y[0] = a[2];

}
```

Appendix D

Function-R-Brake

```
/*
The required channel data are indicated below:
a[0]: eDrive Torque
a[1]: Transmission Ratio of Single Ratio Transmission
a[5]: brake pressure input
a[11]: Brake Piston Surface-Rear
a[12]: Specific Brake Factor- Rear
a[13]: Efficiency- Rear
a[14]: Effective Friction Radius
a[15]: Friction Coefficiency- Rear
a[16]: Battery SOC
a[17]: Supercapacitor SOC
y[0]: brake pressure output
*/
if (a[0] < 0&&(a[16]<90 || a[17]<80))
{
   eBrake = 2*a[0]*a[1]/(2*a[11]*a[13]*a[14]*a[14]*a[15]);
}
else
{
    eBrake = 0.;
}

if ((eBrake+a[5])>0.0)
```

```
{
    y[0]= (eBrake+a[5]);
}
```

Appendix E

Function-DCDC

```
/*
The required channel data are indicated below:
a[0]: Brake Pressure
a[1]: Velocity
a[2]: Battery SOC
a[3]: Ultracapacitor SOC
y[0]: Switch Output
*/
if(a[0]>0 && a[1]>0.1)
{
if(30<a[2]<90)
{
y[0]=-1;
sleep(0.001);
}
else
{
y[0]=0;
}
}
```

else

{

if(50<a[3]<90)

{

y[0]=1;

sleep(0.001);

}

else

{

y[0]=0;

}

}

Appendix F

Function-Range Extender

*/**

The required channel data are indicated below:

a[0]: Battery SOC

a[1]: Lower Bound of SOC

a[2]: Upper Bound of SOC

a[3]: Range Extender Start-witch input

a[4]: Engine speed

a[5]: Engine Load

a[6]: Desired engine

a[7]: Real Time

y[0]: Start-switch of Alternator

y[1]: Alternator Load

```
y[2]: Start-switch of Engine
y[3]: Engine Load
*/
int  operatingMode;
if(a[7]<=0.0) { operatingMode = 0; }
if (a[0] <=  a[1] )
{
  operatingMode=1;
}
if  (a[0] >=  a[2] )
{
  operatingMode=0;
}
if (operatingMode)
{
   y[0] = 1;
   y[1] = 0;
   if (a[4]> (a[6]-50))
   {
      y[1] = -0.5;
    }
   y[2] = a[3];
   y[3] = a[5];
    if ( (a[4]< (a[6]-50)) && (a[5]>0.5) )
   {
      y[3] = 0.5;
```

```
      sleep(0.001);
     }
}
if (!operatingMode)
{
   y[0] = 0.0;
   y[1] = 0.0;
   y[2] = 0.0;
   y[3] = 0.0;
}
```

VITA AUCTORIS

NAME:	Yi Zhang
PLACE OF BIRTH:	Jinan, Shan Dong, China
YEAR OF BIRTH:	1988
EDUCATION:	University of Windsor, MASc, Windsor, ON, 2017